Progress in Surface Science 96 (2021) 100637

Contents lists available at ScienceDirect

Progress in Surface Science

journal homepage: www.elsevier.com/locate/progsurf

Review article

# Advances in two-dimensional heterostructures by mono-element intercalation underneath epitaxial graphene

Songhao Wu [a], Quanzhen Zhang [a], Huixia Yang [a], Yuanxiao Ma [a], Teng Zhang [a], Liwei Liu [a,*], Hong-Jun Gao [b], Yeliang Wang [a,*]

[a] School of Integrated Circuits and Electronics, Beijing Institute of Technology, Beijing 100081, China
[b] Institute of Physics, Chinese Academy of Sciences, Beijing 100190, China

ARTICLE INFO

*Keywords:*
Two-dimensional materials
Epitaxial graphene
Intercalation
Heterostructures

ABSTRACT

Two-dimensional (2D) materials have displayed many remarkable physical properties, including 2D superconductivity, magnetism, and layer-dependent bandgaps. However, it is difficult for a single 2D material to meet complex practical requirements. Heterostructures obtained by vertically stacking different kinds of 2D materials have extensively attracted researchers' attention because of their rich electronic features. With heterostructures, the constraints of lattice matching can be overcome. Meanwhile, high application potential has been explored for electronic and optoelectronic devices, including tunneling transistors, flexible electronics, and photodetectors. Specifically, graphene-based van der Waals heterostructures (vdWHs) by intercalation are emerging to realize various functional heterostructures-based electronic devices. Intercalating atoms under epitaxial graphene can efficiently decouple graphene from the substrate, and is expected to realize rich novel electronic properties in graphene. In this study, we systematically review the progress of the mono-element intercalation in graphene-based vdWHs, including the intercalation mechanism, intercalation-modified electronic properties, and the practical applications of 2D intercalated heterostructures. This work would inspire edge-cutting ideas in the scientific frontiers of 2D materials.

## 1. Introduction

Novel physical properties, for instance, superconductivity and ferromagnetism have been extensively studied in graphene since its discovery [1,2]. Exploration in a wide range of 2D layered materials has promoted the rapid development of surface science. Although high-quality and large-area graphene can be easily fabricated by epitaxial growth, the application of graphene in microelectronic devices is still limited up to now, owing to the absent bandgap [3], negligible spin–orbit interaction (SOI) [4–6], and unavoidable electronic coupling with the substrate [7–10]. Recently, many attempts have been done to improve the electronic properties of graphene. For example, it has been demonstrated that decorating the graphene surface via chemical treatment or deposition of metal atoms can efficiently introduce a band gap of the epitaxial graphene [11,12]. However, due to the instability of the decorated graphene under high temperatures and additional electronic scattering induced by metal atoms, it is almost impossible for practical application [13]. On the other hand, intercalation of the epitaxial graphene has been proven to be a promising strategy to precisely manipulate the electronic properties of graphene [14,15]. Particularly, the intercalation of a mono-element layer between graphene and substrate is

* Corresponding authors.
*E-mail addresses:* liwei.liu@bit.edu.cn (L. Liu), yeliang.wang@bit.edu.cn (Y. Wang).

https://doi.org/10.1016/j.progsurf.2021.100637

Available online 16 July 2021

supposed to construct graphene-based heterostructures. In traditional systems without van der Waals force, the two monolayers have identical crystal structures and lattice constants, which seriously limits the diversity of heterostructures. Constructing graphene-based heterostructures by intercalation, not only can improve many properties of graphene, such as increasing the conductivity, carrier mobility, transparency, and mechanical flexibility [16], but also may lead to new phenomena, for example, superconductivity, spin splitting, magnetic response, thermoelectricity, and spin polarization. In addition, graphene-based vdWHs by intercalation are crucial for both fundamental research [17,18] and practical applications [19–21]. They engender intriguing properties for easy manipulation of the creation, confinement, and transport of charge carriers, excitons, photons, and phonons [22–25].

The geometric structures and electronic properties of graphene-based vdWHs by intercalation are determined by many factors, such as substrate [26], temperature [27], and especially the intercalated atoms [28]. Promisingly, a vast number of diverse heterostructures with unique functionalities are likely to be obtained by extensive varieties of intercalated atoms [29–31]. Therefore, we classify the elements according to the groups or functions of the intercalated atoms in this review, as illustrated in Fig. 1. For example, alkali/alkaline earth metal intercalation induces superconductivity, lanthanide metal intercalation tunes the doping of graphene to n-type, and magnetic metal intercalation realizes various magnetic responses. In addition, semiconductor element intercalation widens the bandgap of graphene.

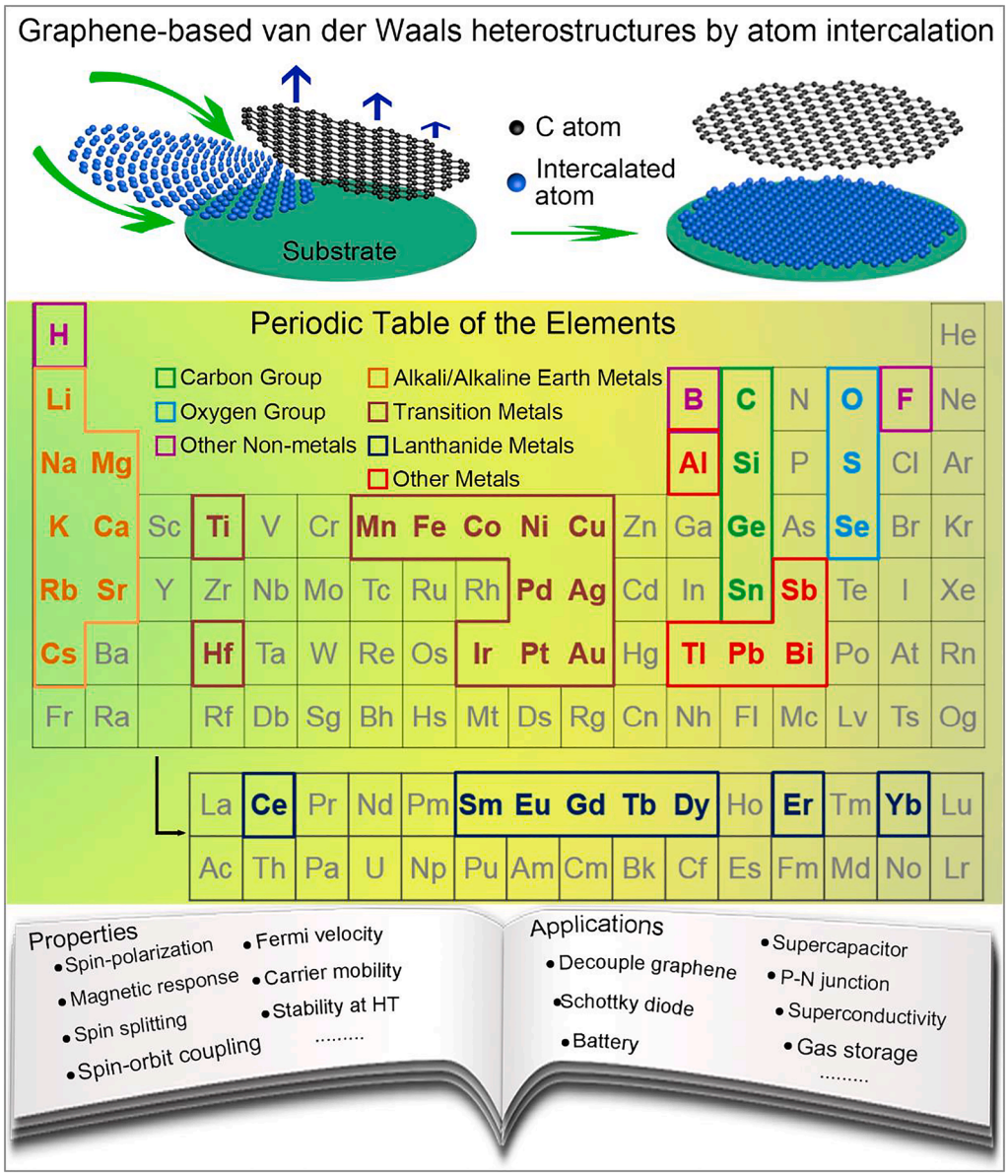


**Fig. 1.** The topic of this review. The elements, which have been used for intercalation under epitaxial graphene, are marked in the periodic table of elements and classified into several groups.

In this review, we firstly give a brief introduction to the main intercalation mechanisms. Secondly, the novel electronic properties that arise from vdWHs by intercalation of different atoms are discussed in detail. We primarily focus on the interfaces, defects, edges, bandgap, Fermi velocity, and carrier mobility of the graphene-based vdWHs, using a variety of techniques of scanning tunneling microscopy (STM), angle-resolved photoemission spectroscopy (ARPES), low-energy electron diffraction (LEED), and Raman spectroscopy. Next, novel applications that have been developed from these graphene-based vdWHs are introduced. Finally, a perspective on the ability of graphene-based vdWHs is promoted for the development of fundamental research and practical applications.

## 2. Intercalation mechanisms by atoms

Intercalation behavior can be affected by various factors, and especially the intercalated atoms play a significant role in tuning the electronic properties of the graphene-based heterostructures [32]. Although intercalation has been widely investigated both theoretically and experimentally [33,34], its precise mechanism has not been clear yet. Here, we introduce four main types of intercalation mechanisms: (1) diffusion through edges [35], (2) penetration through layer [36,37], (3) intercalation through pre-existing defects or metal atom-aided defect [38,39], and (4) exchange mechanism [40,41].

Fig. 2(a) depicts the diffusion process of intercalation through graphene edges. Gas-phase precursors, such as $H_2$, $O_2$, $F_2$, can achieve intercalation in this way [42,43]. For example, Ma *et al.* found that oxygen molecules could be easily adsorbed and dissociate into radical pairs on bare Cu(1 1 1) or Ni(1 1 1) surfaces at near or below room temperature [44]. The precursor atoms subsequently diffuse on the substrate surface and attach to the edges of graphene. Atoms continually pass through the edges, and gradually grow into a monolayer. Graphene is simultaneously decoupled from the substrate and its intrinsic electronic properties are restored. Several opinions regarding the diffusion positions of atoms have been reported. Bignardi *et al.* reported that the regions of graphene unaligned with the substrate were prioritized during intercalation at 470 K, and those regions retained atoms during the deintercalation [35]. Carlos *et al.* thought that atomic intercalation started from the metal step edges at ~ 550 K, which were covered by graphene [45]. To conclude, atoms intercalation by diffusion occurs through either zigzag or armchair graphene edges by overcoming a small energy barrier.

Fig. 2(b) illustrates the process of penetration intercalation. First, perfect monolayer graphene is grown on a metal surface, which is followed by the deposition of atoms on the top of graphene through atomic evaporation. After that, annealed atoms gradually penetrate the graphene film to form nanoislands on the metal surface, eventually growing into a monolayer. Besides above mentioned bottom-up synthesis method, the top-down penetration method is also exploited. Meng *et al.* fabricated graphene/silicon(Si) layered

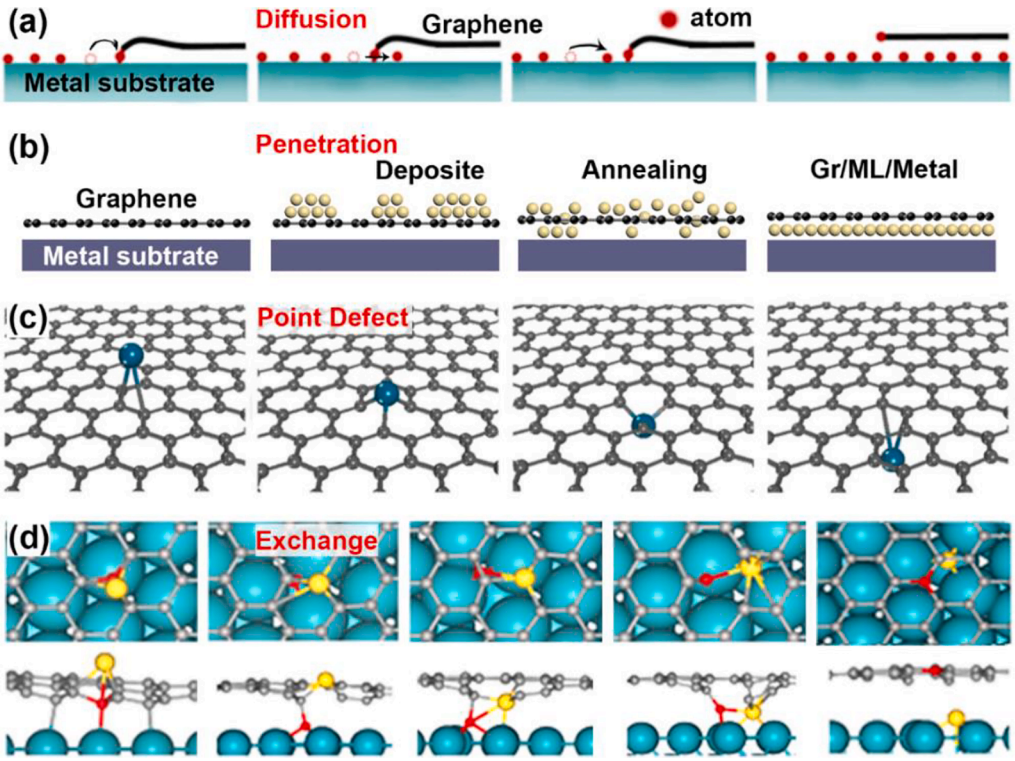


**Fig. 2.** Mechanisms of intercalation under graphene. (a) Diffusion process. (b) Penetration process. (c) Metal atom-aided defect formation. (d) Exchange process. (a) Reproduced with permission. [44] Copyright 2015 American Chemical Society. (c) Reproduced with permission. [39] Copyright 2011 American Institute of Physics. (d) Reproduced with permission. [41] Copyright 2012 Tsinghua University Press and Springer-Verlag Berlin Heidelberg.

heterostructures on the surface of an iridium (Ir) substrate [46]. In the fabrication process, firstly the Ir substrate is pretreated by depositing carbon atoms. Then, Si atoms are evaporated to the surface of the Ir(1 1 1) substrate. After annealing, the disordered Si atoms become regular Si films, and carbon atoms gradually permeate through the Si film, aggregating to form monolayer graphene on top of the Si film.

The third intercalation mechanism involves defects. Fig. 2(c) illustrates an intercalation process through atom-aided defect formation. This intercalation mechanism is applicable for most metal atoms, such as noble metals, magnetic metals, IIIA group metals, and rare earth metals [39]. This process occurs as follows: metal atoms are deposited on perfect graphene, dispersing randomly on the graphene surface. After annealing, metal atoms locally break C–C bonds and combine with carbon atoms, creating an atomic adatom defect in graphene. These defects serve as windows so that the metal atoms can pass through the graphene and intercalate into the graphene/substrate interface. As a result, metal atoms gradually aggregate to form a monolayer. Finally, graphene self-heals the damaged C–C bonds and reverts them to their original state. Zhao *et al.* studied single-Fe atom intercalation using density functional theory (DFT) [47]. They found that once a single Fe atom created such an atomic defect and crossed the defect, the subsequent intercalations become easier, because of the increased pore size of the defect.

The fourth one is an exchange-based mechanism, which is like atom-aided defect formation and recovery. As depicted in Fig. 2(d), it is also an intercalation process about creating a point defect. The difference is that the intercalated atom reacts with C atoms to produce a new compound. Defective graphene may be used to promote intercalation over large areas. Cui *et al.* believed that Si atoms intercalated graphene through this mechanism [41]. In the case of Si intercalation, Si atom is situated at the graphene face-centered cubic (FCC) site and presses C atom down. After annealing at 900 K, the Si atom overcomes the first barrier and occupies the position where it pushes the C atom to the metal surface. Subsequently, the Si atom continues to subside, and the Si and C atoms form a

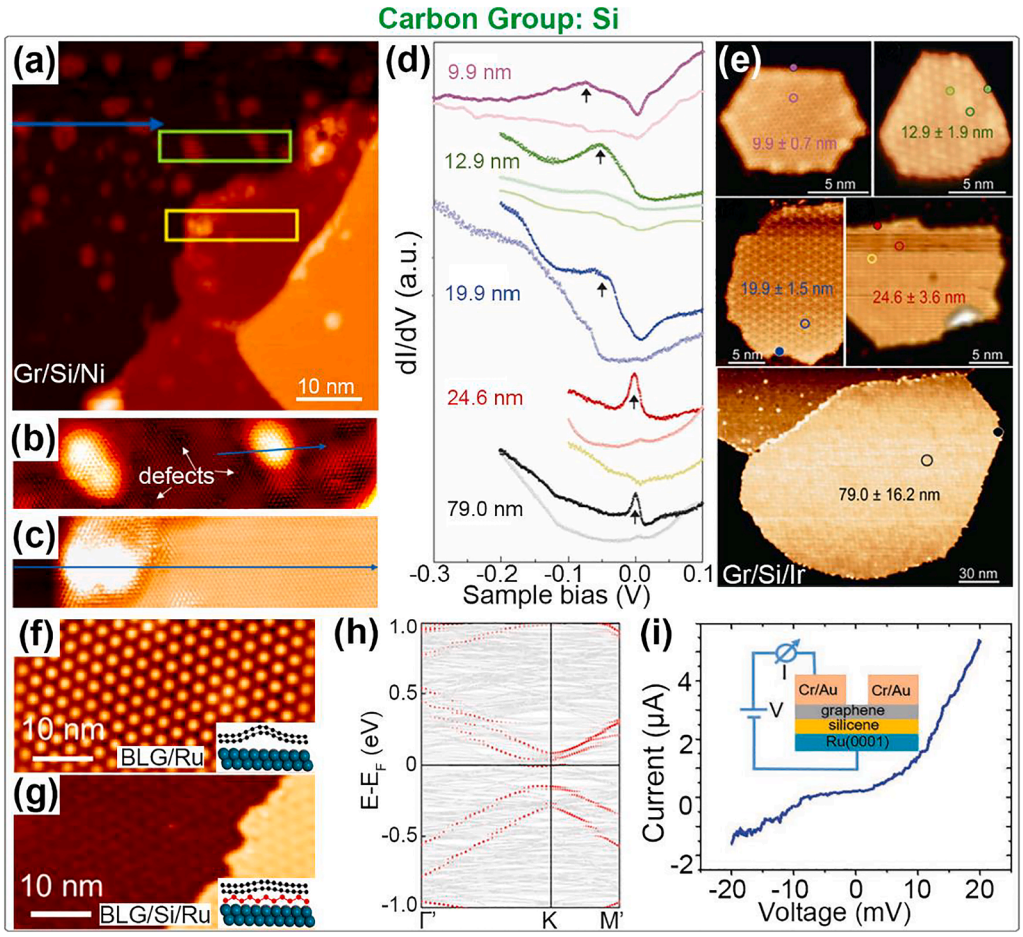


**Fig. 3.** Intercalation with Si atoms. (a–c) STM images of the Si intercalated Gr/Ni(1 1 1) sample. (d, e) Size-dependent edge states of the graphene nanoislands. (f, g) STM images of bilayer graphene (BLG)/Ru and BLG/Si/Ru. (h) Calculated band structure based on the structure of BLG/Si/Ru. The red dots are the band projected on the BLG and the gray lines are the bands of the whole system. (i) The I-V curve of the Gr/Si/Ru heterostructure. (a–c) Reproduced with permission. [49] Copyright 2019 Elsevier Ltd. (d, e) Reproduced with permission. [50] Copyright 2017 Tsinghua University Press and Springer-Verlag GmbH Germany, part of Springer Nature. (f–h) Reproduced with permission. [15] Copyright 2020 American Chemical Society. (i) Reproduced with permission. [51] Copyright 2018 WILEY-VCH Verlag GmbH & Co. KGaA, Weinheim. (For interpretation of the references to colour in this figure legend, the reader is referred to the web version of this article.)

metastable Si-C dimer on the substrate surface, creating a monovacancy of graphene. Finally, the C atom moves upward to repair the monovacancy, and the Si atom intercalates the surface between graphene and substrate through a rotation of the Si-C dimer. As a result, the graphene film is recovered although the Si atoms intercalate the interface of graphene and the substrate.

## 3. Two-dimensional heterostructures by non-metal atom intercalation

### 3.1. Intercalation with carbon group atoms

Intercalants are expected to tailor the electronic properties of graphene (Gr) to meet the specific demand for applications. Group-IV semiconducting elements such as Si, germanium (Ge), and tin (Sn) are easily intercalated by deposition and post-annealing. Moreover, semiconductor elements probably widen the bandgap of graphene owing to their large bandgap offsets [48].

It has been demonstrated that Si acts as a buffer layer enabling graphene to recover the intrinsic electronic structure, while after annealing some intercalated Si atoms may react with the substrate to form strong covalent bonds [41,49]. Here, we introduce several typical works to explore the detailed intercalation process and electrical properties of the Gr/Si heterostructures on metal substrates.

The positions of Si intercalation are studied. Meng *et al.* reported the fabrication of Gr/Si heterostructures on the surface of Ir(1 1 1) after annealing at 800 K [52]. After annealing, they found that intercalation took place preferentially at the edges and the terraces. A very recent study demonstrated that Si atoms also penetrate epitaxial graphene even at room temperature [49]. As shown in Fig. 3 (a–c), Si clusters are randomly distributed on terraces and the step edges with the same height without post-annealing, and some defects evenly surround the Si clusters. It can be concluded that the Si intercalation starts both at the step edges and on the terraces

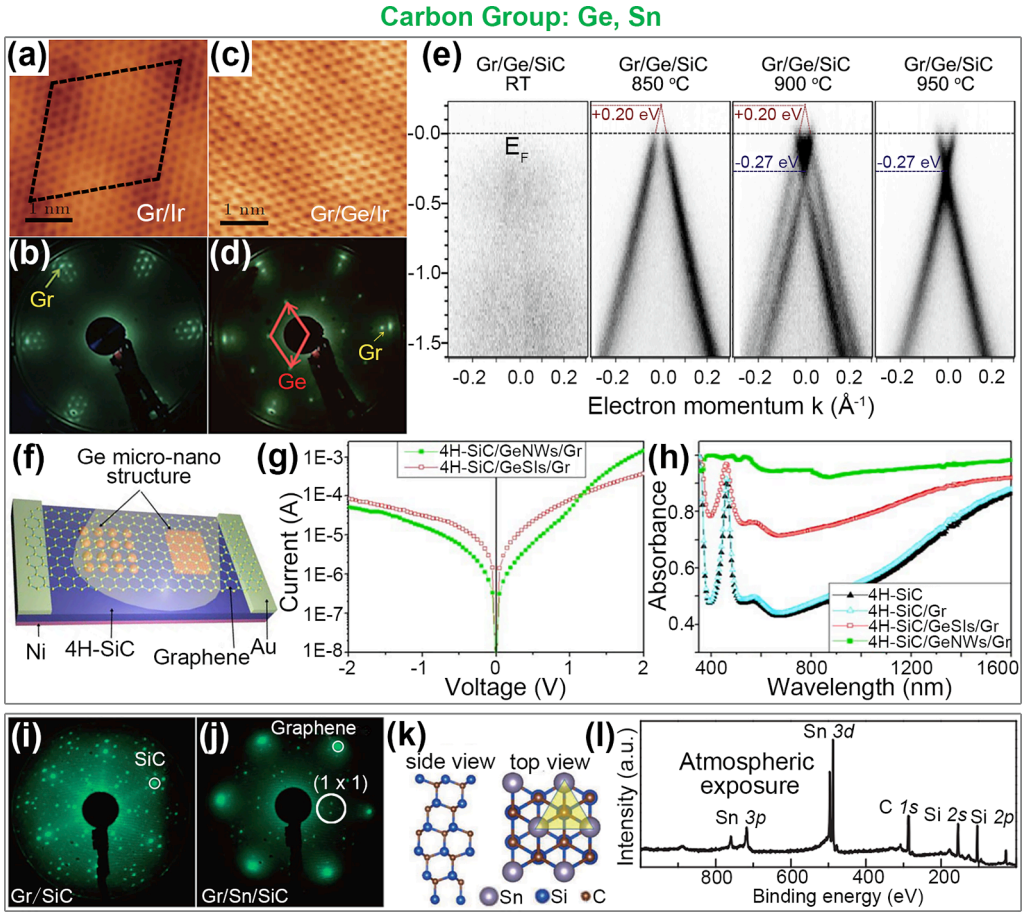


**Fig. 4.** Intercalation of Ge and Sn under graphene. (a–d) STM images and LEED patterns for samples before and after Ge intercalation under graphene on Ir(1 1 1). (e) ARPES results of the initial deposition and after annealing of Ge at T = 850 °C, 900 °C, and 950 °C, respectively. (f) Schematic diagram of Gr/Ge/4H-SiC heterostructure device and the dimension is 5 mm × 5 mm. (g, h) Rectification characteristic and visible (VIS)-near-infrared (NIR) transmittance spectra of this device. (i, j) LEED patterns of Gr/SiC before and after Sn intercalation. (k) A triangular lattice atomic layer of Sn model. (l) X-ray photoelectron spectroscopy (XPS) data of Sn-intercalated graphene exposure at atmosphere. (a-d) Reproduced with permission. [58] Copyright 2019 Chinese Physical Society and IOP Publishing Ltd. (e) Reproduced with permission. [59] Copyright 2016 Elsevier Ltd. (f–h) Reproduced with permission. [60] Copyright 2020 IOP Publishing Ltd. (i–l) Reproduced with permission. [61] Copyright 2018 the Japan Society of Applied Physics.

after annealing.

Apart from the process of Si intercalation, the electronic structure of Gr/Si heterostructure also has attracted much attention. Spin-polarized edge-states are predicted to exist in graphene nanoislands (GNI) with well-defined zigzag edges [53]. However, the edge states of GNIs on metal substrates are not observed, which might be due to the strong interaction with the substrate [54]. Very interesting, the edge states of GNIs are observed by intercalating a Si monolayer between graphene and the metal substrate. Deniz *et al.* synthesized armchair graphene nanoribbons on Au(1 1 1) and found some width-dependent edge states after Si intercalation underneath graphene [9]. Chen *et al.* also successfully recovered the edge states of graphene by intercalating Si between graphene and the Ir (1 1 1) substrate [50]. As shown in Fig. 3(d, e), they found that the edge states of the GNI could shift to the Fermi level with increasing size due to the quantum confinement effect.

Studies also demonstrated that Si intercalation would introduce a bandgap in bilayer graphene (BLG). BLG with Si intercalated induces a sizeable bandgap [55,56]. As shown in Fig. 3(f–h), Guo *et al.* fabricated high-quality BLG and Si-intercalated BLG on Ru (0001). The moiré pattern indicates that the BLG is rippled, but after Si intercalation, it becomes smoother. They found that the vdWHs of Si-intercalated BLG induced a bandgap (0.2 eV), making it promising as a high-mobility channel material. They concluded that the bandgap was caused by a cooperative effect of electron doping and rippling [15].

Gr/Si/metal heterostructures have many potential applications. For example, Li *et al.* explored the current–voltage (I-V) characteristics of these heterostructures and found a Schottky-like rectification behavior, which is especially important for practical application in micro/nano-electronic devices [51]. The inset of Fig. 3(i) displays the device structure and its measurement setup. These heterostructures also show no obvious damage after air exposure up to two weeks, indicating good air stability. To enable easier compatibility with the current Si-based microelectronic techniques, Que *et al.* prepared a single-crystalline Ir(1 1 1) film on a bulk Si substrate for easy preparation of epitaxial graphene, followed by intercalation of Si atoms as a buffer layer between graphene and Ir (1 1 1) to form Gr/Si/metal heterostructures. This method is a new strategy towards the fabrication and especially the integration of graphene-based devices on Si-based substrate [57].

Although Si atoms can be directly intercalated into the graphene-metal interface, Si intercalation only induces n-type doping of graphene [62]. In addition, it has been reported that Ge intercalations also happen for graphene grown both on metal and SiC substrates. The Ge intercalations could even induce doping from p-type to n-type. Ge and Sn atoms are heavy than Si atoms, possessing great potential in microelectronics technology owing to their special electronic properties, such as light trapping effect [60], and large bandgap offsets [63].

Several heterostructures of Gr/Ge and Gr/Sn are reviewed here in detail. Fig. 4(a) illustrates the atomically resolved honeycomb lattice of defect-free graphene on Ir(1 1 1). The black dashed-rhombus is used to label the corresponding unit cell of the moiré pattern of graphene on Ir(1 1 1). Owing to the mismatched lattice between graphene and Ir(1 1 1), a few sharp spots and surrounding satellite spots of graphene appear in LEED patterns, as shown in Fig. 4(b). This suggests that the fabricated graphene is a single crystal material without extra diffraction. After Ge intercalation, as shown in Fig. 4(c, d), the atomically resolved honeycomb structure of graphene appears without a moiré pattern. The corresponding diffraction spots of graphene in the LEED pattern are still clear, while the satellite spots become blurry, revealing that the interaction of graphene with its substrate is weakened. Moreover, The new spots of Ge superstructure indicate that the Ge atoms are successfully intercalated at the Gr/Ir interface [58].

Although Ge atoms successfully intercalate the Gr/metal or Gr/SiC interface, the mechanism of ambipolar doping (p-type doping and n-type doping) is inconsistent. Fig. 4(e) displays the electronic band structure around the $K^{-}$ point of the Ge intercalated graphene Brillouin zone, which is used to describe the correlation [59]. No graphene-like π bands appear at the stage of initial 1/3 Ge buffer layer intercalation. After 4-monolayer Ge intercalation, the π bands of graphene appear. The decoupled graphene exhibits three phases under the influence of annealing temperature (p-type, T = 850 °C; p- and n-type, T = 900 °C; n-type, T = 950 °C). Kim *et al.* thought that such a transition from p-type to n-type was associated with the strong correlation of electrons, which existed between the first and the second Ge interfacial layers. Emtsev *et al.* proposed that ambipolar doping depends on the amount of intercalated Ge atoms [64]. Similarly, Konstantin *et al.* propounded that the ambipolar doping was due to the different thicknesses of the Ge intercalation, which resulted from the annealing temperature [62].

The intercalation of Ge under graphene has been widely used in devices. For example, the Gr/Ge vertical heterostructure is used as a switching device, by using the p- and n-type doping of epitaxial graphene with intercalation of Ge [65,66]. Konstantin *et al.* prepared a p-n junction by Ge intercalation on SiC(0001) [62]. The Gr/Ge/SiC heterostructure, as a near-infrared absorption layer, is used to widen the detection of the wavelength range and increase the detection sensitivity of optoelectronic devices [60]. Nano-scaled Ge structures are sensitive to the near-infrared owing to the narrow bandgap of Ge. This photodetector was prepared on 4H-SiC by using the molecular beam epitaxy method, as shown in Fig. 4(f). The photodetector shows excellent absorbance, which is 90% in the 500–1600 nm range, and the rectification ratio reaches 25 ± 2 V due to the large carrier mobility in Ge, as illustrated in Fig. 4(g, h).

Graphene grown epitaxially on Si-terminated SiC, exhibits reduced carrier mobility due to the strong interaction of graphene with the substrate. Interesting, epitaxial graphene on Si-terminated SiC can be converted into quasi-free-standing monolayer graphene with weakening interlayer interaction by Sn intercalation to form a buffer layer of $SnSi_x$ [67]. It can be achieved to increase the carrier mobility of graphene by intercalating Sn into the graphene/SiC interface [68]. Shingo *et al.* reported that Sn intercalation occurred at the Gr/Si-terminated SiC interface, as shown in Fig. 4(i–l) [61]. The brightness of the diffraction spots of graphene increases, suggesting that the Sn intercalation decouples the buffer layer. Meanwhile, a new type of Sn atomic layer (1 × 1) appears, which is caused by the Sn interface structure. The Sn atoms occupied the on-top sites of Si-terminated SiC(0001), resulting in a triangular lattice and contact with each other by in-plane Sn-Sn bonding. The Sn triangular lattice atomic layer exhibits strong resistance to oxidation. The O 1 s signal is not detected after atmospheric exposure, indicating that the Sn-intercalated interface is chemically inert, which would be useful for device fabrication.

In addition to the graphene/SiC interface, the intercalation of Sn into the graphene/metal interface has also been studied. Ni(1 1 1) is considered the closest lattice match with graphene (~1.2%) of all transition metals. The separation of Ni substrate and graphene is ~ 2.2 Å, indicating that there is a strong interaction between Ni substrate and graphene. Addou *et al.* pointed out that the Sn intercalation and Ni substrate could form an ordered surface alloy after annealing, and the surface alloy could effectively decouple graphene because of the weak interaction between Sn and graphene. Moreover, the case of Sn intercalated graphene on Ni(1 1 1) displays excellent stability, which is caused by the formation of Sn-Ni surface alloy [69].

### 3.2. Intercalation with oxygen group atoms

It is generally a challenging task to achieve free-standing graphene from the substrate because of its strong interaction [70,71]. Elements of group VIA have a stronger ability to combine with metals than carbon, so oxygen group atoms are considered as a low-damage and reliable way to decouple graphene from Rh(1 1 1) [72]. As shown in Fig. 5(a), experimental observations provide direct evidence for the oxygen intercalation. The areas located above the metallic steps of the substrate are considered as the active sites for oxygen intercalation to the Gr–metal interface [45].

Oxygen group atoms could also lead to heavily p-doped graphene, which has been experimentally and theoretically confirmed [73]. Fig. 5(b) presents an intuitive insight into the electronic structure before and after oxygen intercalation. Before intercalation, the graphene displays two banding energies due to the strong hybridization, which promotes the graphene π band to the lower binding energy. Oxygen intercalation is performed by exposing the sample to molecular oxygen at a temperature of about 200–220 °C. The main Dirac cone is shifted upwards, and the mini-cone feature disappears owing to the hybridization of carbon pz orbitals and cobalt d band [74]. However, Li *et al.* claimed that the intercalated oxygen was molecular. The disappearance of the oxygen signal (blue dotted line in Fig. 5(c)) indicates oxygen desorbs at 800 K. They thought it would require a much higher temperature to remove chemisorbed oxygen atoms from the metal [75].

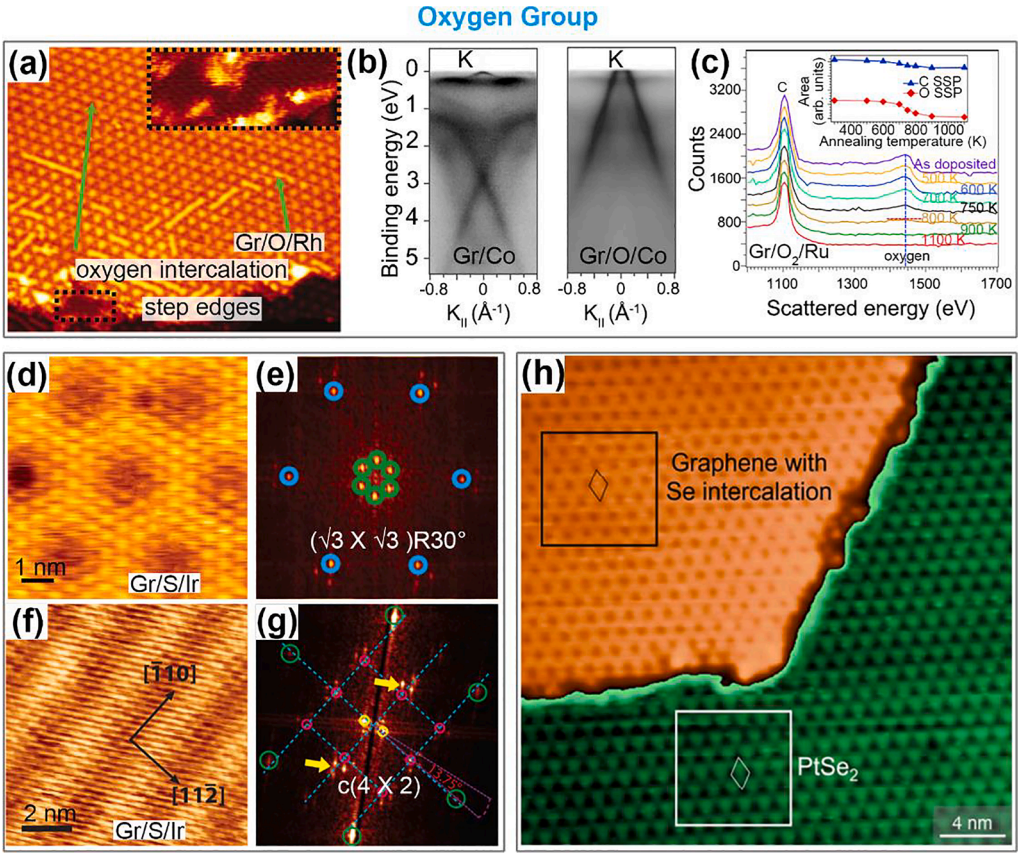


**Fig. 5.** Intercalation with oxygen group atoms. (a) STM image of intercalated Gr/O/Rh(1 1 1) surface. (b) Momentum maps of pristine Gr/Co and oxygen intercalated region. (c) Spectra at a scattering angle of 115° and the inset is the as-prepared Gr/$O_2$/Ru. (d–g) STM images and corresponding Fourier Transform (FT) images of Sulfur (S) intercalation under graphene. (h) STM topographic images of the selenium (Se) intercalation. (a) Reproduced with permission. [45] Copyright 2018 the Owner Societies. (b) Reproduced with permission. [74] Copyright 2020 Elsevier Ltd. (c) Reproduced with permission. [75] Copyright 2017 American Physical Society. (d–g) Reproduced with permission. [76] Copyright 2020 American Chemical Society. (h) Reproduced with permission. [77] Copyright 2020 Tsinghua University Press and Springer-Verlag GmbH Germany, part of Springer Nature.

Sulfur (S) intercalation is an efficient strategy that alters the surface structures during the growth of graphene on metal [78]. Borna *et al.* studied S-intercalated graphene on Ir(1 1 1) and obtained two superstructures using two kinds of precursors ($H_2S$ and $FeS_2$), as shown in Fig. 5(d–g) [76]. In addition to tuning the surface structure, S intercalation has other potential applications. It has been reported that binary doping of S and N into graphene layers could enhance the electrochemical performance of supercapacitors [79]. Heterostructures of S-doped graphene can also be used as high-performance anodes for batteries [80]. In the case of Se intercalation, Liu *et al.* reported that Se was intercalated under graphene on the Pt substrate without formation of $PtSe_2$, although monolayer $PtSe_2$ can be formed on bare Pt [77], as shown in Fig. 5(h). That is, the graphene coverage prevents the selenization of Pt substrate.

### 3.3. Intercalation with other non-metal atoms

As a non-metallic element, boron with great flexibility is a good conductor of heat and electricity. Borophene (B), with a 2D superlattice form of boron, has a high in-plane anisotropy, which is due to its different in-plane bonding. Boron is trivalent, which enables it to take on many 2D phases that bond to substrates through van der Waals interaction without lattice matching. Therefore, Boron can be easily integrated into various 2D heterostructures [81,82].

Kochaev *et al.* studied heterostructures of B/Gr by DFT and found excellent elastic properties [83]. The chemical activity of boron is strong, resulting in the easy reaction with acids, alkalis, metals, *etc.* Hence, it is difficult to prepare 2D layered Boron. Fortunately, monolayer B is prepared by intercalating boron atoms in graphene [81]. As shown in Fig. 6(a, b), Liu *et al.* first evaporated carbon from a graphite rod to prepare submonolayer graphene on a single-crystal Ag(1 1 1) substrate at 750 °C. A monolayer Boron was subsequently prepared by electron beam evaporation of boron. In fact, there are three typical regions, that is, borophene, graphene, and borophene-intercalated graphene. We focus on the areas of B-intercalated graphene. The more refined STM image suggests that borophene successfully intercalates graphene, and Gr/B heterostructures are prepared. Fig. 6(c, d) reveal a continuous graphene lattice

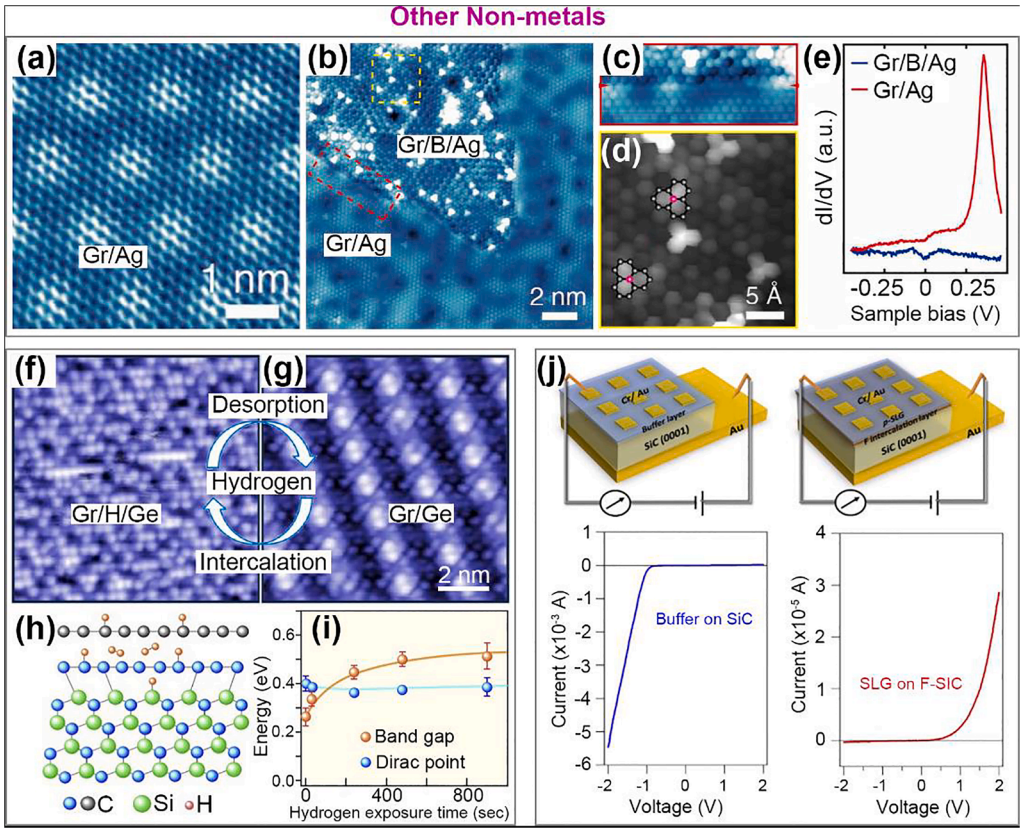


**Fig. 6.** Intercalation with other non-metal atoms. (a, b) STM topography images of as-grown and borophene-intercalated graphene domain on Ag (1 1 1). (c, d) Two zoomed-in STM images of the graphene/borophene interface (red arrowheads) and borophene-intercalated graphene domain (yellow dashed) from (b). (e) Point STS spectra of graphene and borophene-intercalated graphene (stabilized at Vs = −0.1 V, It = 100 pA). (f, g) Hydrogen (H) intercalation and desorption graphene on Ge(1 1 0). (h) Schematic crystal structure of hydrogen intercalated SiC. (i) The relationship of bandgap and Dirac point as a function of hydrogen-exposure time. (j) Scheme of the SiC Schottky diode and two I–V characteristics of buffer/SiC and p-SLG/SiC with Cr contacts. (a–e) Reproduced with permission. [81] Copyright 2019 American Association for the Advancement of Science. (f, g) Reproduced with permission. [85] Copyright 2018 American Chemical Society. (h, i) Reproduced with permission. [86] Copyright 2017 Elsevier Ltd. (j) Reproduced with permission. [87] Copyright 2018 Elsevier Ltd. (For interpretation of the references to colour in this figure legend, the reader is referred to the web version of this article.)

across the interface and a honeycomb lattice of graphene on the triangular domains, which have been marked in Fig. 6(d). Compared with Gr/Ag(1 1 1) (red curve), the d*I*/d*V* spectra of Gr/B/Ag (blue curve) lack a high local density of states (LDOS) feature, which is the Shockley surface state of Ag(1 1 1) [84], as shown in Fig. 6(e). This evidence suggests that Boron decouples graphene from the Ag(1 1 1) substrate.

Hydrogen intercalation, which can generate an H-terminated Ge(1 1 0) surface, is used to control the surface reconstruction of Ge (1 1 0) under graphene [85], as illustrated in Fig. 6(f, g). The reconstruction is a reversible process, which arose from hydrogen intercalation or desorption. The controllable and reversible hydrogen passivation on Ge(1 1 0) provides profound information to inspire the controllable synthesis of other hydrogen-passivated 2D materials, such as phosphorene and antimonene. Hydrogen intercalation under graphene is a typical way to functionalize graphene. Besides, the hydrogen intercalation on Ir(1 1 1) is investigated as a diffusion mechanism [42] and will introduce p-type doping (~0.28 eV) [88]. Moreover, it has been shown that chemical functionalization with hydrogen could turn graphene into a gapped semiconductor [89].

Though the buffer layer on SiC possesses some novel properties, it inevitably limits the carrier mobility of graphene. Hydrogen intercalation is considered an effective method for decoupling the buffer layer on SiC, since the formation of Si-H bonds is more energetically favorable than Si-C bonds [90]. Shtepliuk et *al.* successfully converted the buffer layer to a quasi-free-standing monolayer on SiC via hydrogen intercalation [91].

The intercalation of hydrogen into SiC could also be used to store hydrogen [86]. As shown in Fig. 6(h, i), some hydrogen atoms combine with Si and C, and some hydrogen molecules remain in the buffer layer. The bandgap gradually increases with the longer hydrogen-exposure time, and almost saturate at 240 s. It suggests that there is a correlation between the two essential physical

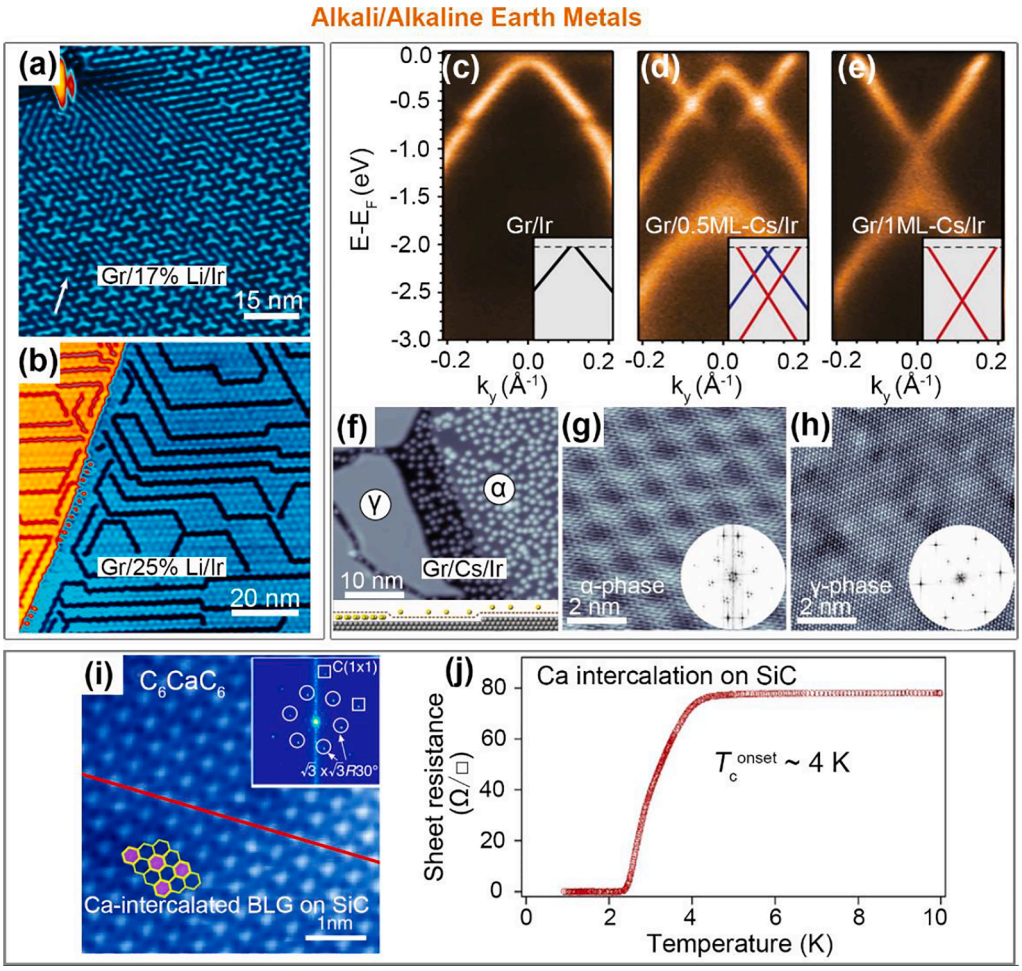


**Fig. 7.** Intercalation with alkali/alkaline earth metal atoms. (a, b) STM images of Li intercalated graphene at Li coverage of 17% and 25%, respectively. (c–e) ARPES maps of Cs intercalation. The electronic states of Gr/Ir have a sharp Dirac cone and are in a p-doping state (c). As Cs coverage increases, the Dirac cone shifts to higher binding energy, and the electronic state gradually becomes n-doping (d, e). (f–h) STM images of the Cs intercalation. The α-phase (g) and the γ-phase (h). (i) STM images of calcium (Ca)-intercalated BLG on SiC. The hexagons represent the C honeycomb lattice, and Ca atoms locate at the center of colored hexagons. (j) Superconductivity of Ca-intercalated graphene. (a, b) Reproduced with permission. [94] Copyright 2016 American Chemical Society. (c-h) Reproduced with permission. [96] Copyright 2013 Macmillan Publishers Limited. (i) Reproduced with permission. [97] Copyright 2012 PNAS. (j) Reproduced with permission. [98] Copyright 2019 Elsevier Ltd.

parameters (hydrogen-exposure time and bandgap of graphene), which might be beneficial for hydrogen-storage studies.

Fluorinated graphene is the thinnest insulator. It is stable at high temperatures and has excellent mechanical properties, owing to the strong interaction between Fluorine (F) and C [92]. Fluorine intercalation is an inexpensive and continuous method to prepare fluorinated graphene with a direct gas–solid reaction. Fan *et al.* successfully prepared fluorinated graphene with an ultrahigh interlayer distance by fluorine intercalation, and the fluorinated graphene showed excellent self-lubricating ability [93]. Fluorine intercalation could also convert the buffer layer on an intrinsic Si-terminated SiC substrate to p-type single-layer graphene (p-SLG) [87]. This structure of p-SLG/SiC can be used as a complementary SiC Schottky diode. As shown in Fig. 6(j), there are two diode structures: metal/SiC and p-SLG/SiC. Two I–V characteristics suggest that both diodes can be turned on, resulting from carrier injection from the metal or p-SLG to the SiC substrate.

## 4. Two-dimensional heterostructures by metal atom intercalation

### 4.1. Intercalation with alkali/alkaline earth metal atoms

Lithium (Li) is a popular element in alkali earth metals used for intercalations. Moreover, Li intercalation could induce an interesting geometric structure and create a pronounced effect on the electronic structure of graphene. As depicted in Fig. 7(a, b), there are two high-resolution STM images of Li intercalated graphene to study the influence of Li coverage. The insufficient number of Li atoms causes this regular line arrangement, leaving the dark lines not affected [94]. It was found that the anisotropic strain in graphene determines the adsorption geometry of the Li atoms, which creates the preferred intercalation regions. Halle *et al.* found that the intercalated region under low Li coverage would facilitate further intercalation, because the previous intercalation position of dots and stripes started to coalesce with increasing Li coverage.

It has been reported that intercalation alkali/alkaline earth metals can effectively tune the charge-carrier density of the graphene [95]. As shown in Fig. 7(c–e), three different electronic states of graphene before and after cesium (Cs) intercalation are revealed. Intercalation of Cs atoms could also induce two characteristic areas (γ-phase and α-phase). As shown in Fig. 7(f–h), Petrovic *et al.* found that intercalation preferentially occurred in the defects of graphene wrinkles at the Ir(1 1 1) step edge, and was regulated by the weak van der Waals interaction [96]. The more detailed STM characterizations of the two phases clearly show the graphene unit and weak moiré superstructures. These clear STM images indicate that graphene wrinkle defects serve as penetration sites for intercalating atoms.

As a typical example of tuning electronic states, superconductivity induced by alkali/alkaline earth metal intercalation has attracted great attention. In 2012, Profeta *et al.* theoretically proposed that the decoration of graphene with alkali atoms could induce superconductivity [99]. In the same year, Kanetani *et al.* successfully intercalated Ca into bilayer graphene grown on 6H-SiC. They thought that Ca atoms were situated at the center of C honeycomb lattice, and predicted the superconductivity of this structure, as shown in Fig. 7(i) [97]. Until 2015, Ludbrook *et al.* experimentally proved that a Li-decorated graphene monolayer was superconducting, with $T_c \sim 5.9$ K [100]. Soon after, Tiwari *et al.* also observed superconductivity ($T_c \sim 7.4$ K) in Li-intercalated few-layer-graphene [101]. Subsequently, more possible superconductivity with other alkali/alkaline earth metal intercalation was explored. In 2016, Ichinokura *et al.* observed a zero-resistance state at Ca-intercalated bilayer graphene on SiC ($T_c \sim 2$ K) [102]. As shown in Fig. 7(j), the resistance drops steeply at 4 K and reaches zero at 2.2 K. The atomic structure of superconducting Ca-intercalated bilayer graphene is investigated to identify the relationship between superconductivity and Ca atomic arrangement. Endo *et al.* conformed that Ca atoms intercalated into the interface of graphene bilayer and SiC substrate, rather than between two graphene layers [98].

Alkali metal intercalation can also induce regioselective chemical reactivity [103]. Mitchell *et al.* investigated the intercalation of three kinds of alkali metal atoms (Li, Na, and K) on the same metal surface and found that the extent of regioselective chemical reactivity is related to the size of the alkali atom (K > Na > Li). Moreover, heterostructures with alkali metal intercalation can be used as energy storage, especially in alkali metal batteries [104,105]. In the case of batteries, alkali metal ions enter the heterostructures through intercalation, and the excellent performance of battery is because of its large specific surface areas. Shi *et al.* proposed a heterostructure of graphene and Si for lithium/sodium-ion batteries [106]. This structure contains a large specific surface area, which can provide a large reaction interface to store alkali atoms and transmit electrons, and exhibits high mechanical stiffness to the main structural integrity.

### 4.2. Intercalation with magnetic metal atoms

Ferromagnets are the primary materials for ultra-high-density magnetic memories. However, the availability of high-quality monolayer films could greatly improve their development. An ideal solution to achieve this is to deposit ferromagnets at the interface between graphene and the substrate to create monolayer film [107]. Here, we review several intercalations of magnetic atoms to investigate their magnetic responses in detail.

Pacilé *et al.* studied the changes in structural and electronic properties by intercalating magnetic elements (a Ni monolayer) into the graphene/Ir(1 1 1) interface, creating a lattice-mismatched Gr/Ni/Ir(1 1 1) heterostructure [110]. The electronic structure of graphene is converted from nearly undisturbed to a strongly hybridized graphene π-band. Li *et al.* studied the mechanism of Ni intercalation and found that Ni intercalation on Ru(0001) was dominated by an exchange of Ni and C atoms [111].

Intercalation of Co atoms under graphene on Ir(1 1 1) can generate a Co film with adjustable magnetic direction. The Gr/Co interface possesses a strong interface magnetic anisotropy, which is sensitive to laser illumination, external electric field, or current lines [112]. Decker *et al.* also studied this heterostructure and observed an out-of-plane easy axis and a site-dependent spin polarization

[107]. Fig. 8(a) depicts the STM of Co-intercalated graphene and reveals that Co preferentially intercalates at the Ir(1 1 1) step edges. They observed a site-dependent variation of the graphene local effective spin polarization, which had a ferromagnetic coupling at the top sites and antiferromagnetic coupling at the fcc/hcp sites, as shown in Fig. 8(b, c). They claimed that the variation was caused by site-dependent magnetization of the graphene.

The capping graphene layer not only prevents oxidation of the Co, but also increases the upper limit for the perpendicular magnetic anisotropy (PMA), as shown in Fig. 8(d, e) [108]. Carlomagno *et al.* found that local-scale anisotropy and out-of-plane magnetic responses were enhanced in the thin film (5 monolayers), but not in the thick film (10 monolayers) after thermal treatment. These findings suggest that there is a close connection between the local structure of Co and the magnetic response, which was regulated by interface effects.

Magnetic responses of iron (Fe) intercalation under graphene are also interesting. Decker *et al.* studied the energy dependence of the d$I$/d$V$ spectra and the giant tunnel magnetoresistance (TMR) of Fe-intercalated graphene, as shown in Fig. 8(f, g) [109]. They found that the spin-resolved d$I$/d$V$ signals demonstrated a difference at valleys. In contrast, the signals exhibited hardly any difference at hills, and the TMR at valleys was higher, reaching 80%. They inferred that the various responses could be caused by the different conductivities of valleys and hills. When the thickness does not exceed a few nanometers, it is an effective way to tune magnetic responses of the intercalated magnetic layer by controlling the film thickness. This makes it possible to form controllable spin polarization of electrons by Fe intercalation.

### 4.3. Intercalation with transition metal atoms

As mentioned above, the intercalation of magnetic atoms introduces novel magic responses. Intercalation with transition metal atoms could also introduce other novel properties of graphene, such as spin–orbit splitting [113,114]. Besides, intercalation of metal atoms to the graphene/metal interface is a promising approach for preventing the degradation of intercalated metal film [108].

The Gr/Copper (Cu)/Ir heterostructure is a good candidate for new concept devices, because it preserves a linear energy dispersion at the Dirac point, which results from the decoupling of Gr from Cu [115]. Intercalation with Cu underneath graphene has many novel properties. For example, it has been reported that superconductors can be synthesized by intercalating Cu into a topological insulator heterostructure [116]. Fig. 9(a) presents the STM image of a Cu intercalated island on Ir(1 1 1). Fig. 9(b, c) depict the electronic structure of Gr/Ir and Gr/Cu/Ir by ARPES. Before intercalation, there is a clear linear dispersion of the graphene $p$ states, corresponding to a slight $p$-doping. After intercalation, the valence band of the graphene layer becomes $n$-doped. Although a linear dispersion of the graphene π band still exists, the 2–4 eV binding energy region becomes complicated due to hybridization between the graphene $p$ and Cu $3d$ states [117].

It has been reported that gold(Au) has exhibited the potential to induce n-type or p-type doping of graphene, which is related to the amount of Au [118]. Hybridization with Au $5d$ states can induce strong SOI in graphene. Marchenko *et al.* considered that the splitting of energy band was induced by graphene p-band hybridization with the Au d-states [119]. Moreover, Au intercalation could reduce the

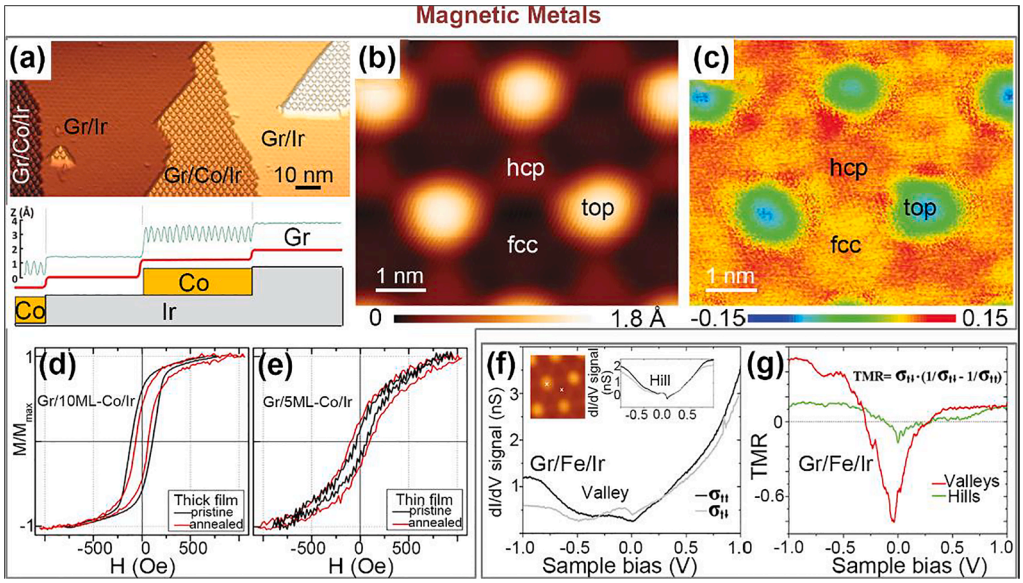


**Fig. 8.** Intercalation with magnetic metal atoms. (a) The topography of the Gr/ cobalt (Co)/Ir surface. (b, c) Local effective spin polarization and corresponding spin asymmetry map of the intercalated graphene layer. (d, e) Out-of-plane magneto-optical Kerr effect signals collected on the thin (d) and thick (e) film. (f) The dI/dV signals of Gr/Fe/Ir at valley and hill. (g) Energy dependence of the tunnel magnetoresistance (TMR). (a–c) Reproduced with permission. [107] Copyright 2013 American Physical Society. (d, e) Reproduced with permission. [108] Copyright 2020 Elsevier B.V. (f, g) Reproduced with permission [109]. Copyright 2014 IOP Publishing Ltd.

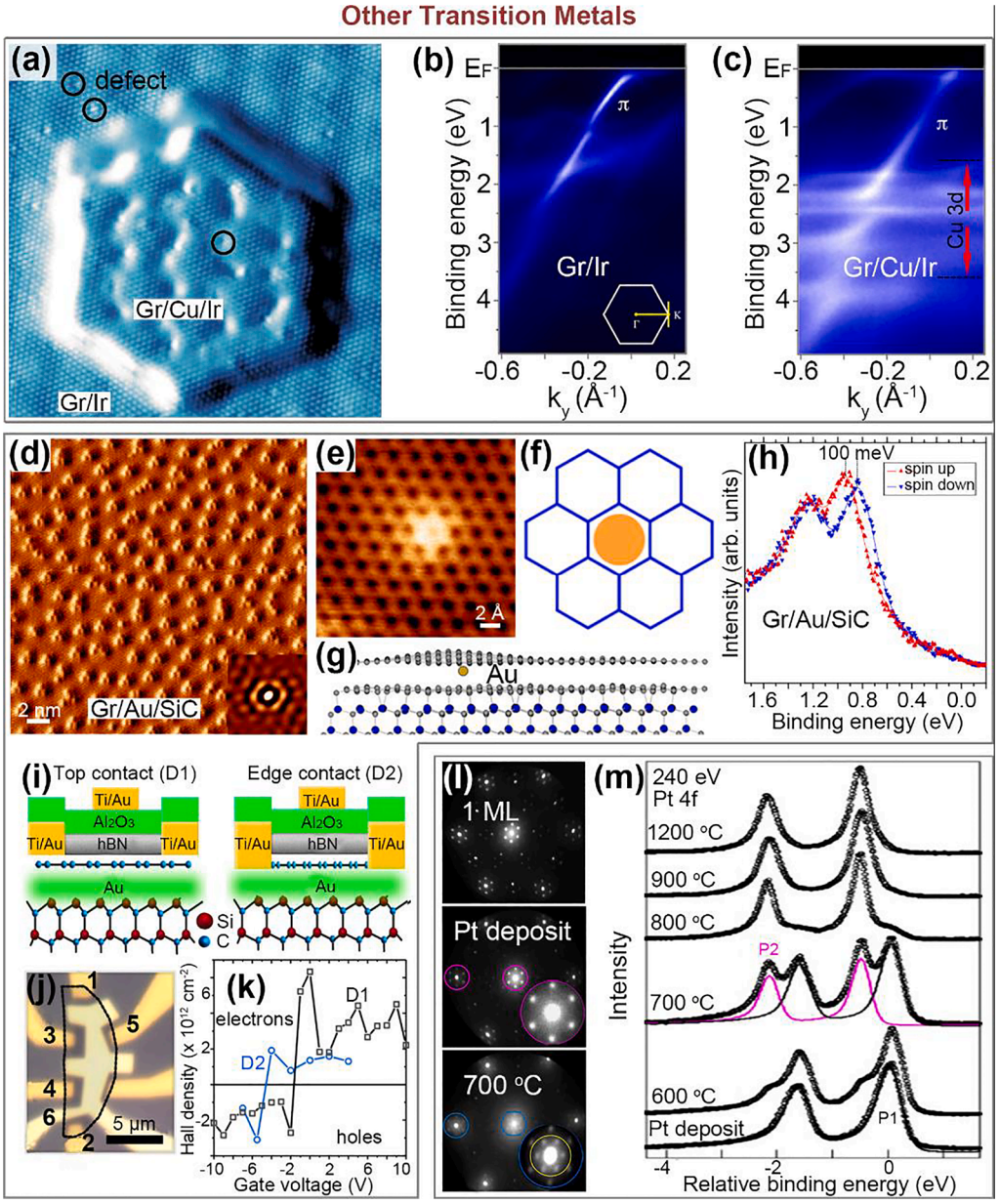


**Fig. 9.** Intercalation with other transition metal atoms. (a) STM images of an intercalated Cu nanoisland. (b, c) Electronic structure of Gr/Ir and Gr/Cu/Ir by ARPES. (d) STM image of the majority of Au dots intercalation Gr/SiC. (e) STM image of an individual Au atom intercalates between the monolayer and the buffer layer. (f, g) Two schematics of the hollow position of the intercalated Au atom. (h) Spin- and angle-resolved photoemission of p-type Au-intercalated graphene on SiC. (i) Schematics of top-gate structures: top contact (D1) and edge contact (D2) configurations. (j) An optical micrograph of D1. (k) Gate-voltage dependence of Hall carrier density of D1 and D2. (l) Selected area LEED patterns of initial 1 ML graphene sample, after platinum (Pt) deposition, after 700 °C annealing. (m) Pt 4f spectra at different temperatures. (a) Reproduced with permission [115]. Copyright 2014 AIP Publishing LLC. (b, c) Reproduced with permission [117]. Copyright 2014 Springer Nature Limited. (d–g) Reproduced with permission. [114] Copyright 2016 American Physical Society. (h) Reproduced with permission, [121] Copyright 2016 the Authors. (i–k) Reproduced with permission. [118] Copyright 2020 Published by the American Physical Society. (l, m) Reproduced with permission. [122] Copyright 2014 the Authors.

restriction of out-of-plane thermal transport of graphene, which is caused by weak van der Waals interactions [120]. Thus, the heterostructures of Gr/Au could be used in various sensitive electronic transmissions or thermoelectric devices.

The intercalation of Au atoms under graphene on C-terminated SiC can form a dispersed phase, as shown in Fig. 9(d). This phase decouples single-layer graphene from SiC without destroying the intrinsic *n*-type doping of graphene, and the Fermi velocity of graphene is increased. These single Au atoms are free-standing and negatively charged. [114]. Fig. 9(e–g) show the STM and

schematics of a single Au atom intercalation, demonstrating that the intercalation position is a hollow position, concerning the six-C atoms of the monolayer graphene. The Au-intercalated *p*-type graphene on SiC displays a 100 meV Rashba-type spin–orbit splitting, and this is the first time that the splitting was induced by graphene p-band hybridization with d-states of the intercalated Au layer on a semiconductor SiC substrate, as seen in Fig. 9(h) [121].

To investigate the electrical properties of the Au-intercalated quasi-free-standing graphene, Kim *et al.* prepared microdevices of the heterostructure [118]. Fig. 9(i, j) present two schematic structures of the top-gated devices (D1 and D2) and an optical micrograph of D1. Through gate-dependent transport measurements, they confirmed that the Au-intercalated buffer layer displayed all the properties of monolayer graphene, namely gate-tunable ambipolar transport across the Dirac point, as shown in Fig. 9(k). They claimed that they found no observable enhancement of SOI in the graphene layer.

Although intercalation can increase the low charge carrier mobility of graphene grown on Si-face SiC [64], intercalation usually is not stable at high temperatures. The stability of quasi-free-standing graphene at high temperatures is a requisite of graphene-based devices. Pt intercalation provides a feasible way to increase stability at high temperatures [122]. Fig. 9(l) exhibits a typical diffraction pattern of monolayer graphene grown on Si-face SiC. This diffraction pattern contains contributions from the ordered graphene layer, SiC substrate, and reconstructed ordered carbon buffer. After the deposition of Pt, the spots intensity from the substrate and the buffer layer decreased but was still detectable. After annealing at 700 °C, six additional superstructure spots appeared, indicating Pt successfully intercalated the surface between SiC and graphene.

Pt intercalation was supposed to passivate the substrate and increase the stability of the graphene at high temperatures. A series of Pt 4f spectra in the XPS measurements of the samples were collected. The Pt 4f core-level spectra shift to higher binding energy after annealing at temperatures higher than 600 °C, as depicted in Fig. 9(m). This demonstrates that there exist high quality and stability quasi-free-standing bilayer graphene and an ordered Pt silicide at the interface.

### 4.4. Intercalation with lanthanide metal atoms

The tiny SOI (<1 μeV) splitting at the Dirac point of graphene limits its development for spintronic devices. The elements in the lanthanide (La) family can usually provide heavy electronic doping of graphene to increase the SOI of graphene[125]. For example, Kim *et al.* studied intercalation of Cerium (Ce), one of the most abundant lanthanides, into Gr/SiC(0001). They found that Ce intercalation can increase the spin degree of freedom to the π-electrons, and thereby strongly enhance the SOI [126]. In addition, they found that there was a temperature-dependent transition, which opened the bandgap (Eg = 0.5 eV) at 41 K, and reduced the bandgap

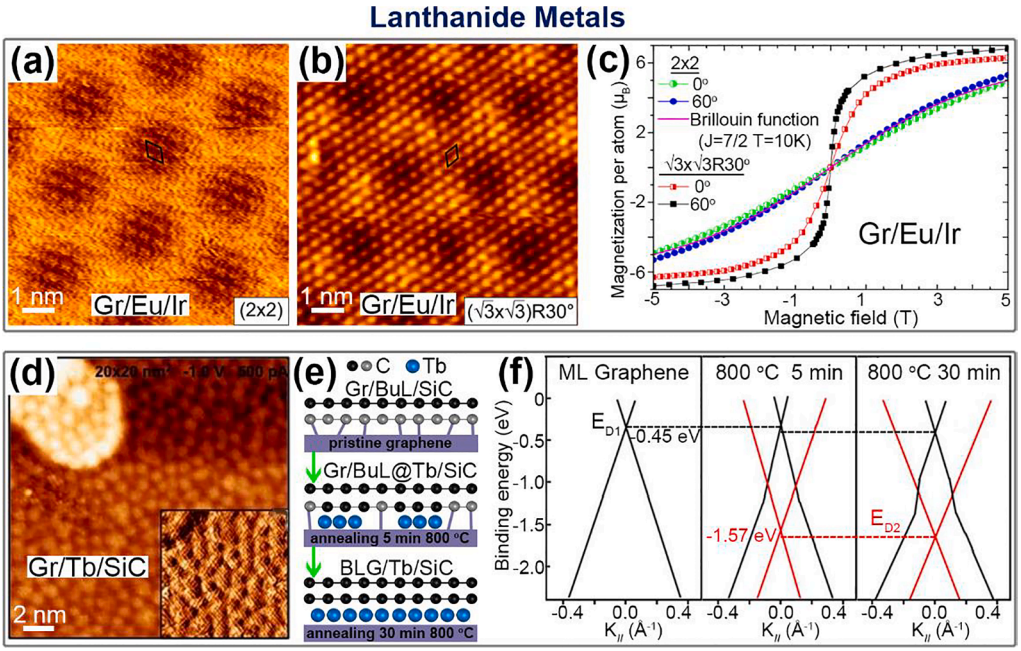


**Fig. 10.** Intercalation with lanthanide (La) atoms. (a, b) STM images of two structures of Europium (Eu) intercalation. (c) Magnetization loops for (2 × 2) and ($\sqrt{3} \times \sqrt{3}$)*R*30° Eu layers at 10 K. (d) STM image of Terbium (Tb) intercalation under graphene on SiC, and the zoom-in image in the inset showed all carbons in graphene lattice. (e) Scheme for Tb intercalated bilayer graphene on SiC(0001). Intercalation of Tb atoms (blue) below a pure buffer layer (BuL, black) leads to the formation of bilayer graphene(BLG). (f) Schemes for an increase in the Fermi surface with the annealing time. $E_{D1}$ is the Dirac point of initial graphene layer, and $E_{D2}$ is a Dirac point located 1.57 eV below the Fermi level, originated from the new layer of graphene. (a–c) Reproduced with permission. [123] Copyright 2014 American Physical Society. (d, f) Reproduced with permission. [124] Copyright 2018 American Physical Society. (For interpretation of the references to colour in this figure legend, the reader is referred to the web version of this article.)

gradually to 0.36 eV with the temperature increasing to room temperature.

Lanthanide atoms possess negligible paramagnetic properties at room temperature. However, at low temperatures, most of the lanthanides are ferromagnetic, which arises from the unfilled 4f electron orbitals [127]. Studies have demonstrated that intercalation of lanthanide under graphene could induce graphene magnetic responses that depend on the different intercalation structures [123]. Schumacher *et al.* demonstrated the different intercalated superstructures of an element of Europium (Eu) underneath graphene on Ir (1 1 1), that is, (2 × 2) and ($\sqrt{3} \times \sqrt{3}$)$R30^o$ concerning graphene, as shown in Fig. 10(a, b). The (2 × 2) superstructure exhibits obvious linear paramagnetic behavior, as the magnetic field changes, but the ($\sqrt{3} \times \sqrt{3}$)$R30^o$ superstructure exhibits a nonlinear magnetic response and is almost saturated at 5 T, as shown in Fig. 10(c). The authors claimed that magnetic coupling was affected by the Ruderman-Kittel-Kasuya-Yosida interaction under graphene, which led to a paramagnetic (2 × 2) intercalation superstructure [128].

There is a complex electronic band structure for most of the metal intercalation of epitaxial graphene on the C-terminated surface of SiC, which displays a mixture of a new linear highly n-doped dispersion and the dispersion of pristine monolayer graphene. However, no systematic studies prove whether the new band structure results from the buffer layer or the monolayer graphene when atoms are intercalated into SiC.

The intercalation of terbium (Tb) makes this problem clear. Terbium intercalation under the buffer layer of the C-terminated surface of SiC(0001) can induce highly n-type doped graphene [124]. Fig. 10(d) presents the STM image of Tb intercalation on SiC, and the inset illustrates all the carbon atoms in the graphene lattice. The disordered intercalation suggests that the (6 × 6)-SiC reconstruction of the buffer layer has disappeared, thus the buffer layer has been completely decoupled from the substrate. Fig. 10(e)

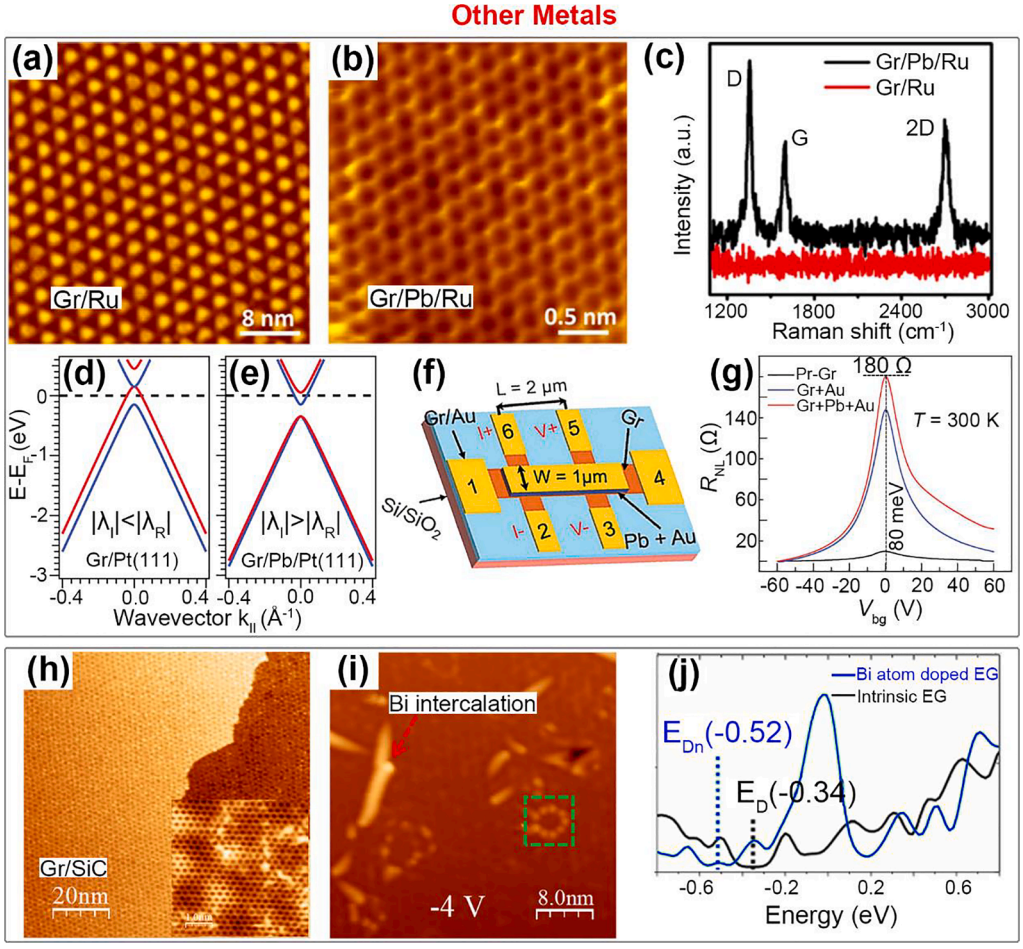


**Fig. 11.** Intercalation with other metal atoms. (a–c) STM images and Raman shifts of Gr/Ru and Gr/Pb/Ru. (d, e) Model band structures of ARPES spectra of Gr/Pt as well as Gr/Pb/Pt after Pb intercalation, obtained at $I\lambda_l I < I\lambda_R I$ (d) and $I\lambda_l I > I\lambda_R I$ for (e). (f) Optical image of the microdevice to detect electrical characteristics of the Gr/Pb/Au heterostructure. In non-local measurement, a current between electrodes 6 and 2 is applied and the voltage drop between 5 and 3 is perceived. For local measurement, a current between electrodes 1 and 4 is applied and the voltage drop between 2 and 3 is detected. (g) Comparison of non-local signal in pristine Gr, Gr/Au, and Gr/Pb/Au. (h, i) STM images of Gr/SiC and bismuth (Bi) intercalated Gr/SiC. (j) Local density of states of the intrinsic epitaxial graphene and Bi intercalated epitaxial graphene. (a–c) Reproduced with permission. [130] Copyright 2015 American Chemical Society. (d, e) Reproduced with permission. [129] Copyright 2016 American Chemical Society. (f, g) Reproduced with permission. [131] Copyright 2019 the Royal Society of Chemistry. (h-j) Reproduced with permission. [132] Copyright 2018 Author(s).

describes the detailed process of how Tb intercalation decouples ML graphene to BLG on SiC. The two Fermi surfaces also prove the formation of BLG, as shown in Fig. 10(f), two dispersion curves (red and black lines) are explained by the superposition of two distinct graphene layers. The Fermi surfaces of the new graphene monolayer increase with the annealing time, which suggests the intercalation of Tb atoms leads to the formation of a new graphene monolayer.

### 4.5. Intercalation with other metal atoms

For application purposes, it is essential to control the bandgap of graphene. The bandgap depends on two fundamental appearance mechanisms: the symmetry breaking of the sublattice and strong SOI induced by intercalation or hybridization with heavy atoms. Graphene can be modified into a narrow-gap semiconductor or a 2D topological insulator by tuning the bandgap with heavy metal intercalation.

It has been reported that Lead (Pb) intercalation can effectively decouple graphene [129]. As shown in Fig. 11(a, b), before Pb intercalation, the monolayer graphene on Ru shows a periodic moiré pattern (~3 nm) due to the lattice mismatch. After Pb intercalation, a perfectly flat honeycomb lattice of graphene with a lattice constant (2.46 ± 0.02 Å) can be observed, which is consistent with free-standing monolayer graphene. As shown in Fig. 11(c), compared with Gr/Ru, the G and 2D peaks in Raman spectra are obvious after the Pb intercalation. This indicates that the coupling between graphene and the substrate is weak, and the intrinsic electronic properties of graphene are restored after the Pb intercalation [130].

In the case of Gr/Pb/Ir, Calleja e*t al.* discovered regular resonances in STS spectra. Such electronic resonances are not present in either monolayer Pb or graphene, however, the combination of the two materials results in such resonances. They interpreted that the Pb monolayer intercalation induced resonances by a strong and spatially modulated SOI [133].

In the case of Gr/Pb/Pt, Klimovskikh *et al.* studied the bandgap modifications after Pb intercalation [129]. A bandgap of ~ 200 meV at the Dirac point of graphene was generated after Pb intercalation, as depicted in Fig. 11(d, e). They claimed that graphene was p-doped before Pb intercalation, however, the graphene transformed to n-doping after Pb intercalation. The conversion of p-doping to n-doping of graphene after Pb intercalation led to a partial occupation of the $\pi^*$ state of graphene, probably due to charge transfer from Pb film to graphene.

Graphene-based vdWHs are possible routes for enhancing the SOI and inducing topological nontrivial gaps near the Dirac point of graphene [134]. Afzal *et al.* prepared a heterostructure of a field-effect transistor by Pb intercalation into the graphene–Au interface, as shown in Fig. 11(f). They measured the current–voltage signals and found that the spin Hall effect induced a giant current–voltage signal, and the SOI was increased to 80 meV, as shown in Fig. 11(g) [131].

In the case of Gr/Bi/SiC, Hu *et al.* studied the Bi intercalation during the thermal decomposition of Si-terminated SiC [132]. The SiC substrate is pretreated with Bi flux, and Bi atoms are subsequently incorporated into epitaxial graphene. As shown in Fig. 11(h–j), a typically clean and smooth surface of epitaxial graphene is prepared. After Bi intercalation, there are many small protrusions and depressions, which are caused by Bi intercalation. It is found that the Dirac point shifts away from the Fermi level, indicating that Bi intercalation significantly enhances the n-doping property of epitaxial graphene. A calculation was performed to explore the enhancement of n-doped behavior. In all, the intercalation of heavy atoms underneath graphene generally enhanced the SOI, making graphene as a 2D semiconductor or topological insulator, more attractive for possible spintronic applications.

## 5. Summary and outlook

In this study, we have reviewed various graphene-based vdWHs intercalated by different kinds of atoms. Many vertical heterostructures with unique functionalities are obtained by extensive varieties of intercalated atoms. Integration of graphene into the heterostructure by intercalation provides a strategy to introduce new electronic properties and functionalities. The intercalation not only modifies the undulations of graphene, but also induces electronic structure changes, such as tuned bandgap by semiconductor and non-metals, strong SOI and magnetism by magnetic atoms, enhanced superconductivity by alkali/alkaline earth metals, and even spin Hall effect by heavily lanthanide metals.

In addition, graphene-based vdWHs by intercalation are crucial for fundamental research, for example, for easy generation and manipulation of excitons, photons, and phonons. Evermore, some novel properties are reported although they are still unclear, like 2D topological superconductivity, topological insulator, Majorana fermions, enhanced Mott insulator, *etc.* Further efforts should elucidate the underneath mechanism for these new physical phenomena in graphene-based vdWHs. The intercalation of graphene-based vdWHs conceive many novel physical and chemical properties and are expected to be used extensively in various fields, including sensors, electronics, supercapacitors, and photonics. Undoubtedly, graphene-based vdWHs by intercalation opens up a new dimension for engineering the electronic, magnetic, and optical properties of 2D materials at the atomic level and provides a new platform in the research frontier of 2D materials.

## Acknowledgments

Thanks for the financial support from the Beijing Natural Science Foundation (Nos. Z190006, 4192054), National Key Research and Development Program of China (2020YFA0308800, 2019YFA0308000), National Natural Science Foundation of China (Nos. 61971035, 61901038, 61725107), and the Strategic Priority Research Program of Chinese Academy of Sciences (Nos. XDB30000000).

## References


[1] M.S. Scheurer, Spectroscopy of graphene with a magic twist, Nature 572 (7767) (2019) 40–41.
[2] J.H. Pixley, E.Y. Andrei, Ferromagnetism in magic-angle graphene, Science 365 (6453) (2019) 543.
[3] H. Kum, D. Lee, W. Kong, H. Kim, Y. Park, Y. Kim, Y. Baek, S.-H. Bae, K. Lee, J. Kim, Epitaxial growth and layer-transfer techniques for heterogeneous integration of materials for electronic and photonic devices, Nat. Electron. 2 (10) (2019) 439–450.
[4] D. Khokhriakov, A.M. Hoque, B. Karpiak, S.P. Dash, Gate-tunable spin-galvanic effect in graphene-topological insulator van der Waals heterostructures at room temperature, Nat. Commun. 11 (2020) 3657.
[5] J.W. McIver, B. Schulte, F.-U. Stein, T. Matsuyama, G. Jotzu, G. Meier, A. Cavalleri, Light-induced anomalous Hall effect in graphene, Nat. Phys. 16 (1) (2020) 38–41.
[6] G.R. Artem A.R. Anna M.O. Mikhail V. Oleg Yu I.K. Ilya E.P. Anatoly V.F. Maria V. Vladimir Yu P.R. Igor E. Arthur A. Andrés V.C. Evgueni M.S. Alexer Magneto-Spin–Orbit Graphene: Interplay between Exchange and Spin-Orbit Couplings, Nano Lett. 18 2018 1564 1574.
[7] K.S. Kim, Y. Zhao, H. Jang, S.Y. Lee, J.M. Kim, K.S. Kim, J.-H. Ahn, P. Kim, J.-Y. Choi, B.H. Hong, Large-scale pattern growth of graphene films for stretchable transparent electrodes, Nature 457 (7230) (2009) 706–710.
[8] P.W. Sutter, J.-I. Flege, E.A. Sutter, Epitaxial graphene on ruthenium, Nat. Mater. 7 (5) (2008) 406–411.
[9] O. Deniz, C. Sánchez-Sánchez, T. Dumslaff, X. Feng, A. Narita, K. Müllen, N. Kharche, V. Meunier, R. Fasel, P. Ruffieux, Revealing the electronic structure of silicon intercalated armchair graphene nanoribbons by scanning tunneling spectroscopy, Nano Lett. 17 (4) (2017) 2197–2203.
[10] J. Song, M. Bernien, C.-B. Wu, W. Kuch, Tuning the electronic properties of rotated graphene on Ni(111) by Nickel Carbide Intercalation, J. Phys. Chem. C 120 (3) (2016) 1546–1555.
[11] O. Cretu, A.V. Krasheninnikov, J.A. Rodriguez-Manzo, L. Sun, R.M. Nieminen, F. Banhart, Migration and Localization of Metal Atoms on Strained Graphene, Phys. Rev. Lett. 105 (2010), 196102.
[12] A. Ahmet, L.J. Hak, K.G.K. Wai, O. Barbaros, Enhanced spin-orbit coupling in dilute fluorinated graphene, 2D Mater. 2 (2015), 044009.
[13] M. Yuya, M. Torge, T. Makoto, T. Shinichi, H. Hiroki, B. Fabio, H. Stefan, Correlation between morphology and transport properties of quasi-free-standing monolayer graphene, Appl. Phys. Lett. 105 (2014), 221604.
[14] M. Schulzendorf, A. Hinaut, M. Kisiel, R. Jöhr, R. Pawlak, P. Restuccia, E. Meyer, M.C. Righi, T. Glatzel, Altering the Properties of Graphene on Cu(111) by Intercalation of Potassium Bromide, ACS Nano 13 (5) (2019) 5485–5492.
[15] H. Guo, R. Zhang, H. Li, X. Wang, H. Lu, K. Qian, G. Li, L. Huang, X. Lin, Y.-Y. Zhang, H. Ding, S. Du, S.T. Pantelides, H.-J. Gao, Sizable Band Gap in Epitaxial Bilayer Graphene Induced by Silicene Intercalation, Nano Lett. 20 (4) (2020) 2674–2680.
[16] P. Solís-Fernández, M. Bissett, H. Ago, Synthesis, structure and applications of graphene-based 2D heterostructures, Chem. Soc. Rev. 46 (15) (2017) 4572–4613.
[17] J. Li, X. Yang, Y. Liu, B. Huang, R. Wu, Z. Zhang, B. Zhao, H. Ma, W. Dang, Z. Wei, K. Wang, Z. Lin, X. Yan, M. Sun, B. Li, X. Pan, J. Luo, G. Zhang, Y. Liu, Y. Huang, X. Duan, X. Duan, General synthesis of two-dimensional van der Waals heterostructure arrays, Nature 579 (7799) (2020) 368–374.
[18] K.S. Burch, D. Mandrus, J.-G. Park, Magnetism in two-dimensional van der Waals materials, Nature 563 (7729) (2018) 47–52.
[19] J. He, N. Kumar, M.Z. Bellus, H.Y. Chiu, D. He, Y. Wang, H. Zhao, Electron transfer and coupling in graphene-tungsten disulfide van der Waals heterostructures, Nat. Commun. 5 (2014) 5622.
[20] T. Song, X. Cai, M.W.-Y. Tu, X. Zhang, B. Huang, N.P. Wilson, K.L. Seyler, L. Zhu, T. Taniguchi, K. Watanabe, M.A. McGuire, D.H. Cobden, D. Xiao, W. Yao, X. Xu, Giant tunneling magnetoresistance in spin-filter van der Waals heterostructures, Science 360 (6394) (2018) 1214–1218.
[21] J.W. Liu, Q.L. Ma, Z.Q. Huang, G.G. Liu, H. Zhang, Recent progress in graphene-based noble-metal nanocomposites for electrocatalytic applications, Adv. Mater. 31 (2019) 1800696.
[22] H. Fang, C. Battaglia, C. Carraro, S. Nemsak, B. Ozdol, J.S. Kang, H.A. Bechtel, S.B. Desai, F. Kronast, A.A. Unal, G. Conti, C. Conlon, G.K. Palsson, M.C. Martin, A.M. Minor, C.S. Fadley, E. Yablonovitch, R. Maboudian, A. Javey, Strong interlayer coupling in van der Waals heterostructures built from single-layer chalcogenides, Proc. Natl. Acad. Sci. USA 111 (17) (2014) 6198–6202.
[23] N. Briggs, B. Bersch, Y. Wang, J. Jiang, R.J. Koch, N. Nayir, K. Wang, M. Kolmer, W. Ko, A. De La Fuente Duran, S. Subramanian, C. Dong, J. Shallenberger, M. Fu, Q. Zou, Y.-W. Chuang, Z. Gai, A.-P. Li, A. Bostwick, C. Jozwiak, C.-Z. Chang, E. Rotenberg, J. Zhu, A.C.T. van Duin, V. Crespi, J.A. Robinson, Atomically thin half-van der Waals metals enabled by confinement heteroepitaxy, Nat. Mater. 19 (6) (2020) 637–643.
[24] L. Yin, F. Wang, R.Q. Cheng, Z.X. Wang, J.W. Chu, Y. Wen, J. He, Van der Waals Heterostructure Devices with Dynamically Controlled Conduction Polarity and Multifunctionality, Adv. Funct. Mater. 29 (2019) 1804897.
[25] Z. Zhang, P. Lin, Q.L. Liao, Z. Kang, H.N. Si, Y. Zhang, Graphene-based mixed-dimensional van der waals heterostructures for advanced optoelectronics, Adv. Mater. 31 (2019) 1806411.
[26] K.S. Novoselov, A. Mishchenko, A. Carvalho, A.H. Castro Neto, 2D materials and van der Waals heterostructures, Science 353 (2016) 9439.
[27] X. Zhou, J. Yang, M. Zhong, Q. Xia, B. Li, X. Duan, Z. Wei, Intercalation of two-dimensional layered materials, Chem. Res. Chinese. U. 36 (4) (2020) 584–596.
[28] L. Daukiya, M.N. Nair, M. Cranney, F. Vonau, S. Hajjar-Garreau, D. Aubel, L. Simon, Functionalization of 2D materials by intercalation, Prog. Surf. Sci. 94 (1) (2019) 1–20.
[29] A.K. Geim, I.V. Grigorieva, Van der Waals heterostructures, Nature 499 (7459) (2013) 419–425.
[30] Y. Liu, Y. Huang, X. Duan, Van der Waals integration before and beyond two-dimensional materials, Nature 567 (7748) (2019) 323–333.
[31] H.-F. Wang, C. Tang, Q. Zhang, A review of graphene-based 3D van der Waals hybrids and their energy applications, Nano Today 25 (2019) 27–37.
[32] I. Pís, S. Nappini, F. Bondino, T.O. Menteş, A. Sala, A. Locatelli, E. Magnano, Fe intercalation under graphene and hexagonal boron nitride in-plane heterostructure on Pt(111), Carbon 134 (2018) 274–282.
[33] B. Natalie, M.G. Zewdu, V. Alexander, Z. Tian, W. Ke, D. Ana De La Fuente, B. Brian, B. Timothy, L.K. Kenneth Jr, A.R. Joshua, Epitaxial graphene/silicon carbide intercalation: A minireview on graphene modulation and unique 2D materials, Nanoscale 11 (2019) 15440–15447.
[34] S. Günther, T.O. Menteş, R. Reichhelt, E. Miniussi, B. Santos, A. Baraldi, A. Locatelli, Au intercalation under epitaxial graphene on Ru(0001): The role of graphene edges, Carbon 162 (2020) 292–299.
[35] B. Luca, L. Paolo, D. Matteo, O. Fabrizio, G. Aliakbar, P. Luca, B. Alessandro, L. Rosanna, L. Silvano, Key Role of Rotated Domains in Oxygen Intercalation at Graphene on Ni(111), 2D Mater. 4 (2017), 025106.
[36] S. Vlaic A. Kimouche J. Coraux B. Santos a.N.R. A. Locatelli, Cobalt intercalation at the graphene/iridium(111) interface: Influence of rotational domains, wrinkles, and atomic steps Appl. Phys. Lett. 104 2014 101602.
[37] Y. Orimoto, K. Otsuka, K. Yagyu, H. Tochihara, T. Suzuki, Y. Aoki, Theoretical study of Cu intercalation through a defect in Zero-Layer graphene on SiC Surface, J. Phys. Chem. C 121 (13) (2017) 7294–7302.
[38] C. Romero-Muñiz, A. Martín-Recio, P. Pou, J.M. Gómez-Rodríguez, R. Pérez, Unveiling the atomistic mechanisms for oxygen intercalation in a strongly interacting graphene-metal interface, Phys. Chem. Chem. Phys. 20 (19) (2018) 13370–13378.
[39] L. Huang, Y. Pan, L. Pan, M. Gao, W.Y. Xu, Y.D. Que, H.T. Zhou, Y.L. Wang, S.X. Du, H.J. Gao, Intercalation of metal islands and films at the interface of epitaxially grown graphene and Ru(0001) surfaces, Appl. Phys. Lett. 99 (2011), 163107.
[40] G. Li, H. Zhou, L. Pan, Y. Zhang, L. Huang, W. Xu, S. Du, M. Ouyang, A.C. Ferrari, H.-J. Gao, Role of Cooperative Interactions in the Intercalation of Heteroatoms between Graphene and a Metal Substrate, J. Am. Chem. Soc. 137 (22) (2015) 7099–7103.
[41] Y. Cui, J. Gao, L. Jin, J. Zhao, D. Tan, Q. Fu, X. Bao, An exchange intercalation mechanism for the formation of a two-dimensional Si structure underneath graphene, Nano Res. 5 (5) (2012) 352–360.
[42] E. Grånäs, T. Gerber, U.A. Schröder, K. Schulte, J.N. Andersen, T. Michely, J. Knudsen, Hydrogen intercalation under graphene on Ir(111), Surf. Sci. 651 (2016) 57–61.

[43] S.B. Mishra, S.K. Yadav, D.G. Kanhere, B.R.K. Nanda, Fluorine intercalated graphene: Formation of a two-dimensional spin lattice through pseudoatomization, Phys. Rev. Mater. 4 (2020), 074411.
[44] L. Ma, X.C. Zeng, J. Wang, Oxygen Intercalation of Graphene on Transition Metal Substrate: An Edge-Limited Mechanism, J. Phys. Chem. Lett. 6 (2015) 4099–4105.
[45] C. Romero-Muñiz, A. Martín-Recio, P. Pou, J.M. Gómez-Rodríguez, R. Pérez, Unveiling the atomistic mechanisms for oxygen intercalation in a strongly interacting graphene-metal interface, Phys. Chem. Chem. Phys. 20 (19) (2018) 13370–13378.
[46] L. Meng, Y. Wang, L. Li, H.J. Gao, Fabrication of graphene-silicon layered heterostructures by carbon penetration of silicon film, Nanotechnology 28 (2017), 084003.
[47] P. Zhao, P. Ren, C.J.K.-J. Weststrate, Y. Xu, D.-B. Cao, H. Xiang, J. Xu, Y. Yang, Y.-W. Li, J.W.H. Niemantsverdriet, X. Wen, X. Yu, Intercalation Mechanisms of Fe Atoms underneath A Graphene Monolayer on Ru(0001), J. Phys. Chem. C 122 (40) (2018) 22903–22910.
[48] D. Kaplan, V. Swaminathan, G. Recine, R. Balu, S. Karna, Bandgap tuning of mono- and bilayer graphene doped with group IV elements, J. Appl. Phys. 113 (2013), 183701.
[49] F. Ronci, S. Colonna, R. Flammini, M. De Crescenzi, M. Scarselli, M. Salvato, I. Berbezier, F. Jardali, C. Lechner, P. Pochet, H. Vach, P. Castrucci, High graphene permeability for room temperature silicon deposition: The role of defects, Carbon 158 (2020) 631–641.
[50] H. Chen, Y. Que, L. Tao, Y.-Y. Zhang, X. Lin, W. Xiao, D. Wang, S. Du, S.T. Pantelides, H.-J. Gao, Recovery of edge states of graphene nanoislands on an iridium substrate by silicon intercalation, Nano Res. 11 (7) (2018) 3722–3729.
[51] G. Li, L. Zhang, W. Xu, J. Pan, S. Song, Y. Zhang, H. Zhou, Y. Wang, L. Bao, Y.Y. Zhang, S. Du, M. Ouyang, S.T. Pantelides, H.J. Gao, Stable Silicene in Graphene/Silicene Van der Waals Heterostructures, Adv. Mater. 30 (2018) 1804650.
[52] L. Meng, R.T. Wu, H.T. Zhou, G. Li, Y. Zhang, L.F. Li, Y.L. Wang, H.J. Gao, Silicon intercalation at the interface of graphene and Ir(111), Appl. Phys. Lett. 100 (2012), 083101.
[53] P. Cui Q. Zhang Z. H.B., X.X. Li, W.Y. Wang, Q.X. Li, C.G. Zeng, and Z.Y. Zhang, Carbon Tetragons as Definitive Spin Switches in Narrow Zigzag Graphene Nanoribbons Phys. Rev. Lett. 116 2016 026802.
[54] H.W. Kim, J.Y. Ku, W. Ko, I. Jeon, H. Kwon, S. Ryu, S.-J. Kahng, S.-H. Lee, S.W. Hwang, H. Suh, Strong interaction between graphene edge and metal revealed by scanning tunneling microscopy, Carbon 78 (2014) 190–195.
[55] Y. Zhang, T.T. Tang, C. Girit, Z. Hao, M.C. Martin, A. Zettl, M.F. Crommie, Y.R. Shen, F. Wang, Direct observation of a widely tunable bandgap in bilayer graphene, Nature 459 (7248) (2009) 820–823.
[56] N. Hirofumi, M. Yu-ichiro, O. Atsushi, Band-unfolding approach to moiré-induced band-gap opening and Fermi level velocity reduction in twisted bilayer graphene, Phys. Rev. B 7 (2017) 2790–2799.
[57] Y.D. Que, Y. Zhang, Y.L. Wang, L. Huang, W.Y. Xu, J. Tao, L.J. Wu, Y.M. Zhu, K. Kisslinger, W. Michael, S. Matthias, C.M. Shen, S.X. Du, Y.Q. Liu, H.J. Gao, Graphene-silicon layered structures on single-crystalline Ir(111) Thin Films, Adv. Mater. Interfaces 2 (2015) 1400543.
[58] H. Guo, X.Y. Wang, D.L. Bao, H.L. Lu, Y.Y. Zhang, G. Li, Y.L. Wang, S.X. Du, H.J. Gao, Fabrication of large-scale graphene/2D-germanium heterostructure by intercalation, Chinese Phys. B 28 (2019), 078103.
[59] H. Kim, O. Dugerjav, A. Lkhagvasuren, J.M. Seo, Origin of ambipolar graphene doping induced by the ordered Ge film intercalated on SiC(0001), Carbon 108 (2016) 154–164.
[60] L. Li, Y. Zang, S. Lin, J. Hu, Y. Han, Q. Chu, Q. Lei, H. Chen, Fabrication and characterization of SiC/Ge/graphene heterojunction with Ge micro-nano structures, Nanotechnology 31 (2020), 145202.
[61] S. Hayashi, A. Visikovskiy, T. Kajiwara, T. Iimori, T. Shirasawa, K. Nakastuji, T. Miyamachi, S. Nakashima, K. Yaji, K. Mase, F. Komori, S. Tanaka, Triangular lattice atomic layer of Sn($1 \times 1$) at graphene/SiC(0001) interface, Appl. Phys. Express 11 (2018), 015202.
[62] A.A.Z. Konstantin, V. Emtsev, C. Coletti, S. Forti, U. Starke, Ambipolar doping in quasifree epitaxial graphene on SiC(0001) controlled by Ge intercalation, Phys. Rev. B 84 (2011), 125423.
[63] S. Sonde, B. Chakrabarti, Y. Liu, K. Sasikumar, J. Lin, L. Stan, R. Divan, L.E. Ocola, D. Rosenmann, P. Choudhury, K. Ni, S.K.R.S. Sankaranarayanan, S. Datta, S. Guha, Silicon compatible Sn-based resistive switching memory, Nanoscale 10 (20) (2018) 9441–9449.
[64] K.V. Emtsev, F. Speck, T. Seyller, L. Ley, J.D. Riley, Interaction, growth, and ordering of epitaxial graphene on SiC{0001} surfaces: A comparative photoelectron spectroscopy study, Phys. Rev. B 77 (2008), 155303.
[65] Y. Wang, Z. Ni, Q. Liu, R. Quhe, J. Zheng, M. Ye, D. Yu, J. Shi, J. Yang, J. Li, J. Lu, All-metallic vertical transistors based on stacked dirac materials, Adv. Funct. Mater. 25 (1) (2015) 68–77.
[66] J. Baringhaus, A. Stöhr, S. Forti, S.A. Krasnikov, A.A. Zakharov, U. Starke, C. Tegenkamp, Bipolar gating of epitaxial graphene by intercalation of Ge, Appl. Phys. Lett. 104 (2014), 261602.
[67] Y.R. Niu, A.A. Zakharov, R. Yakimova, Metal-dielectric transition in Sn-intercalated graphene on SiC(0001), Ultramicroscopy 183 (2017) 49–54.
[68] M.E. Dávila, J. Avila, M.C. Asensio, M. Göthelid, U.O. Karlsson, G. Le Lay, Perturbation of Ge(111) and Si(111)$\sqrt{3}\alpha$-Sn surfaces by adsorption of dopants, Surf. Sci. 600 (16) (2006) 3154–3159.
[69] R. Addou, A. Dahal, M. Batzill, Graphene on ordered Ni-alloy surfaces formed by metal (Sn, Al) intercalation between graphene/Ni(111), Surf. Sci. 606 (13-14) (2012) 1108–1112.
[70] V.P. Anna, A.B. Liubov, J. Lin, M.C.L. Lia, F.S. Grégory, Contact angle measurement of free-standing square-millimeter single-layer graphene, Nat. Commun. 9 (2018) 1–7.
[71] Q. Wang, R. Kitaura, S. Suzuki, Y. Miyauchi, K. Matsuda, Y. Yamamoto, S. Arai, H. Shinohara, Fabrication and In Situ transmission electron microscope characterization of free-standing graphene nanoribbon devices, ACS Nano 10 (1) (2016) 1475–1480.
[72] A. Dong, Q. Fu, M. Wei, Y. Liu, Y. Ning, F. Yang, H. Bluhm, X. Bao, Facile oxygen intercalation between full layer graphene and Ru(0001) under ambient conditions, Surf. Sci. 634 (2015) 37–43.
[73] E. Voloshina, N. Berdunov, Y. Dedkov, Restoring a nearly free-standing character of graphene on Ru(0001) by oxygen intercalation, Sci. Rep. 6 (2016) 20285.
[74] M. Jugovac, F. Genuzio, T.O. Menteş, A. Locatelli, G. Zamborlini, V. Feyer, C.M. Schneider, Tunable coupling by means of oxygen intercalation and removal at the strongly interacting graphene/cobalt interface, Carbon 163 (2020) 341–347.
[75] T.B. Li, J.A. Yarmoff, Intercalation and desorption of oxygen between graphene and Ru(0001) studied with helium ion scattering, Phys. Rev. B 96 (2017), 155441.
[76] Borna Pielić Joshua Hall Vito Despoja Iva Šrut Rakić Marin Petrović Ali Sohani Carsten Busse Thomas Michely Marko Kralj 124 12 2020 6659 6668.
[77] Z.L. Liu, Z.-L. Zhu, X. Wu, J.-A. Shi, W. Zhou, L.-W. Liu, Y.-L. Wang, H.-J. Gao, Using graphene to suppress the selenization of Pt for controllable fabrication of monolayer $PtSe_2$, Nano Res. 13 (12) (2020) 3212–3216.
[78] J. Ekspong, R. Sandström, L.P. Rajukumar, M. Terrones, T. Wågberg, E. Gracia-Espino, Stable Sulfur-Intercalated 1T′ $MoS_2$ on Graphitic nanoribbons as hydrogen evolution electrocatalyst, Adv. Funct. Mater. 28 (2018) 1802744.
[79] X. Zhang, P. Yan, R. Zhang, K. Liu, Y. Liu, T. Liu, X. Wang, A novel approach of binary doping sulfur and nitrogen into graphene layers for enhancing electrochemical performances of supercapacitors, J. Mater. Chem. A 4 (48) (2016) 19053–19059.
[80] C.H. Yang, X.H. Liang, X. Qu, Q.B. Zhang, H.S. Zheng, F.H. Zheng, J.H. Wang, K. Huang, M. Liu, Heterostructured Nanocube-Shaped Binary Sulfide (SnCo)S-2 Interlaced with S-Doped Graphene as a High-Performance Anode for Advanced Na+ Batteries, Adv. Funct. Mater. 29 (2019) 1807971.
[81] X.L. Liu, M.C. Hersam, Borophene-graphene heterostructures, Sci. Adv. 5 (2019) 6444.
[82] M. Ou, X. Wang, L. Yu, C. Liu, W. Tao, X. Ji, L. Mei, The emergence and evolution of borophene, Adv. Sci. 8 (12) (2021) 2001801, https://doi.org/10.1002/advs.v8.1210.1002/advs.202001801.
[83] A. Kochaev, K. Katin, M. Maslov, R. Meftakhutdinov, AA-stacked borophene-graphene bilayer with covalent bonding: Ab Initio investigation of structural, electronic and elastic properties, J. Phys. Chem. Lett. 11 (2020) 5668–5673.
[84] M. Marks, A. Schöll, U. Höfer, Formation of metal–organic interface states studied with 2PPE, J. Electron. Spectrosc 195 (2014) 263–271.

[85] D.C. Zhou, Z.Q. Niu, T.C. Niu, Surface Reconstruction of Germanium: Hydrogen Intercalation and Graphene Protection, J. Phys. Chem. C 122 (2018) 21874–21882.
[86] K. Sugawara, K. Suzuki, M. Sato, T. Sato, T. Takahashi, Enhancement of band gap and evolution of in-gap states in hydrogen-adsorbed monolayer graphene on SiC(0001), Carbon 124 (2017) 584–587.
[87] S.Y. Lee, J. Kim, S. Ahn, K.-J. Jeon, H. Seo, Complementary Schottky diode formation with carbon buffer and p-doped single layer graphene on intrinsic SiC via fluorine intercalation, Carbon 142 (2019) 254–260.
[88] R. Balog, A. Cassidy, J. Jorgensen, L. Kyhl, M. Andersen, A.G. Cabo, F. Ravani, L. Bignardi, P. Lacovig, S. Lizzit, L. Hornekaer, Hydrogen interaction with graphene on Ir(1 1 1): a combined intercalation and functionalization study, J. Phys. Condens. Matter 31 (2019), 085001.
[89] J.H. Jørgensen, A.G. Čabo, R. Balog, L. Kyhl, M.N. Groves, A.M. Cassidy, A. Bruix, M. Bianchi, M. Dendzik, M.A. Arman, L. Lammich, J.I. Pascual, J. Knudsen, B. Hammer, P. Hofmann, L. Hornekaer, Symmetry-driven band gap engineering in hydrogen functionalized graphene, Acs Nano 10 (12) (2016) 10798–10807.
[90] J. Soltys, J. Piechota, M. Ptasinska, S. Krukowski, Hydrogen intercalation of single and multiple layer graphene synthesized on Si-terminated SiC(0001) surface, J. Appl. Phys. 116 (2014), 083502.
[91] I. Shtepliuk, I.G. Ivanov, T. Iakimov, R. Yakimova, A. Kakanakova-Georgieva, P. Fiorenza, F. Giannazzo, Raman probing of hydrogen-intercalated graphene on Si-face 4H-SiC, Mat. Sci. Semicon. Proc. 96 (2019) 145–152.
[92] J. Zhao, H. Petek, Non-nuclear electron transport channels in hollow molecules, Phys. Rev. B 90 (2014), 075412.
[93] K. Fan, J. Fu, X. Liu, Y. Liu, W. Lai, X. Liu, X. Wang, Dependence of the fluorination intercalation of graphene toward high-quality fluorinated graphene formation, Chem. Sci. 10 (21) (2019) 5546–5555.
[94] J. Halle, N. Néel, J. Kröger, Filling the Gap: Li-Intercalated Graphene on Ir(111), J. Phys. Chem. C 120 (9) (2016) 5067–5073.
[95] R. Shimizu, K. Sugawara, K. Kanetani, K. Iwaya, T. Sato, T. Takahashi, T. Hitosugi, Charge-density wave in Ca-intercalated bilayer graphene induced by commensurate lattice matching, Phys. Rev. Lett. 114 (2015), 146103.
[96] M. Petrovic, I. Srut Rakic, S. Runte, C. Busse, J.T. Sadowski, P. Lazic, I. Pletikosic, Z.H. Pan, M. Milun, P. Pervan, N. Atodiresei, R. Brako, D. Sokcevic, T. Valla, T. Michely, M. Kralj, The mechanism of caesium intercalation of graphene, Nat. Commun. 4 (2013) 2772.
[97] K. Kanetani, K. Sugawara, T. Sato, R. Shimizu, K. Iwaya, T. Hitosugi, T. Takahashi, Ca intercalated bilayer graphene as a thinnest limit of superconducting $C_6Ca$, Proc. Natl. Acad. Sci. USA 109 (48) (2012) 19610–19613.
[98] Y. Endo, Y. Fukaya, I. Mochizuki, A. Takayama, T. Hyodo, S. Hasegawa, Structure of superconducting Ca-intercalated bilayer Graphene/SiC studied using total-reflection high-energy positron diffraction, Carbon 157 (2020) 857–862.
[99] G. Profeta, M. Calandra, F. Mauri, Phonon-mediated superconductivity in graphene by lithium deposition, Nat. Phys. 8 (2) (2012) 131–134.
[100] B.M. Ludbrook, G. Levy, P. Nigge, M. Zonno, M. Schneider, D.J. Dvorak, C.N. Veenstra, S. Zhdanovich, D. Wong, P. Dosanjh, C. Straßer, A. Stöhr, S. Forti, C. R. Ast, U. Starke, A. Damascelli, Evidence for superconductivity in Li-decorated monolayer graphene, Proc. Natl. Acad. Sci. USA 112 (38) (2015) 11795–11799.
[101] A.P. Tiwari, S. Shin, E. Hwang, S.G. Jung, T. Park, H. Lee, Superconductivity at 7.4 K in few layer graphene by Li-intercalation, J. Phys. Condens. 29 (Matter 2017,), 445701.
[102] S. Ichinokura, K. Sugawara, A. Takayama, T. Takahashi, S. Hasegawa, Superconducting calcium-intercalated bilayer graphene, ACS Nano 10 (2) (2016) 2761–2765.
[103] I. Mitchell, S. Irle, A.J. Page, Inducing regioselective chemical reactivity in graphene with alkali metal intercalation, Phys. Chem. Chem. Phys. 20 (30) (2018) 19987–19994.
[104] A. Yierpan, S. Cem, G. Oğuz, M.P. François, Ç. Deniz, MXenes/graphene heterostructures for Li battery applications: a first principles study, J. Mater. Chem. A 6 (2018) 2337–2345.
[105] G.Z. Li, B. Huang, Z.F. Pan, X.Y. Su, Z.P. Shao, L. An, Advances in three-dimensional graphene-based materials: configurations, preparation and application in secondary metal (Li, Na, K, Mg, Al)-ion batteries, Energy Environ. Sci. 12 (2019) 2030–2053.
[106] L. Shi, T.S. Zhao, A. Xu, J.B. Xu, Ab initio prediction of a silicene and graphene heterostructure as an anode material for Li- and Na-ion batteries, J. Mater. Chem. A 4 (42) (2016) 16377–16382.
[107] R. Decker, J. Brede, N. Atodiresei, V. Caciuc, S. Blügel, R. Wiesendanger, Atomic-scale magnetism of cobalt-intercalated graphene, Phys. Rev. B 87 (2013), 041403.
[108] A.M.S.I. Carlomagnoa, L. Carlinia, J. Drnecb, G. Vinaic, P. Torellic, R. Felicid, S. Mobilioa, C. Meneghini, Evidence of a thermally-induced microstructural anisotropy in Gr/Co/Ir (111) systems, Appl. Surf. Sci. 535 (2020), 146365.
[109] R. Decker, M. Bazarnik, N. Atodiresei, V. Caciuc, S. Blugel, R. Wiesendanger, Local tunnel magnetoresistance of an iron intercalated graphene-based heterostructure, J. Phys. Condens. Matter 26 (2014), 394004.
[110] D. Pacilé, P. Leicht, M. Papagno, P.M. Sheverdyaeva, P. Moras, C. Carbone, K. Krausert, L. Zielke, M. Fonin, Y.S. Dedkov, F. Mittendorfer, J. Doppler, A. Garhofer, J. Redinger, Artificially lattice-mismatched graphene/metal interface: Graphene/Ni/Ir(111), Phys. Rev. B 87 (3) (2013), https://doi.org/10.1103/PhysRevB.87.035420.
[111] J. Li, Q. Fu, Y. Yang, X.H. Bao, A comparative study of intercalation mechanism at graphene/Ru(0001) interface, Surf. Sci. 617 (2013) 81–86.
[112] J. Coraux, A.T. N'Diaye, N. Rougemaille, C. Vo-Van, A. Kimouche, H.-X. Yang, M. Chshiev, N. Bendiab, O. Fruchart, A.K. Schmid, Air-protected epitaxial graphene/ferromagnet hybrids prepared by chemical vapor deposition and intercalation, J. Phys. Chem. Lett. 3 (15) (2012) 2059–2063.
[113] L.F. Li, Y.L. Wang, L. Meng, R.T. Wu, H.J. Gao, Hafnium intercalation between epitaxial graphene and Ir(111) substrate, Appl. Phys. Lett. 102 (2013), 093106.
[114] M. Narayanan Nair, M. Cranney, T. Jiang, S. HajjarGarreau, D. Aubel, F. Vonau, A. Florentin, E. Denys, M.L. Bocquet, L. Simon, Noble-metal intercalation process leading to a protected adatom in a graphene hollow site, Phys. Rev. B 94 (2016), 075427.
[115] M. Sicot, Y. Fagot-Revurat, B. Kierren, G. Vasseur, D. Malterre, Copper intercalation at the interface of graphene and Ir(111) studied by scanning tunneling microscopy, Appl. Phys. Lett. 105 (2014), 191603.
[116] S. Satoshi, S. Kouji, A. Yoichi, Superconductor derived from a topological insulator heterostructure, Phys. Rev. B 90 (2014), 220504.
[117] H. Vita, S. Bottcher, K. Horn, E.N. Voloshina, R.E. Ovcharenko, T. Kampen, A. Thissen, Y.S. Dedkov, Understanding the origin of band gap formation in graphene on metals: graphene on Cu/Ir(111), Sci. Rep. 4 (2014) 5704.
[118] K.H. Kim, H. He, C. Struzzi, A. Zakharov, C.E. Giusca, A. Tzalenchuk, Y.W. Park, R. Yakimova, S. Kubatkin, S. Lara-Avila, Ambipolar charge transport in quasi-free-standing monolayer graphene on SiC obtained by gold intercalation, Phys. Rev. B 102 (2020), 165403.
[119] D. Marchenko, A. Varykhalov, M.R. Scholz, G. Bihlmayer, E.I. Rashba, A. Rybkin, A.M. Shikin, O. Rader, Giant Rashba splitting in graphene due to hybridization with gold, Nat. Commun. 3 (2012) 1232.
[120] Z. Juang, C. Tseng, Y. Shi, W. Hsieh, S. Ryuzaki, N. Saito, C. Hsiung, W. Chang, Y. Hernandez, Y. Han, K. Tamada, L. Li, Graphene-Au nanoparticle based vertical heterostructures: A novel route towards high- ZT Thermoelectric devices, Nano Energy 38 (2017) 385–391.
[121] D. Marchenko, A. Varykhalov, J. Sánchez-Barriga, T. Seyller, O. Rader, Rashba splitting of 100 meV in Au-intercalated graphene on SiC, Appl. Phys. Lett. 108 (2016), 172405.
[122] C. Xia, L.I. Johansson, Y. Niu, A.A. Zakharov, E. Janzén, C. Virojanadara, High thermal stability quasi-free-standing bilayer graphene formed on 4H–SiC(0 0 0 1) via platinum intercalation, Carbon 79 (2014) 631–635.
[123] S. Schumacher F. Huttmann M. Petrović C. Witt D.F. Förster C. Vo-Van J. Coraux A.J. Martínez-Galera V. Sessi I. Vergara R. Rückamp M. Grüninger N. Schleheck F. Meyer zu Heringdorf, P. Ohresser, M. Kralj, T.O. Wehling, and T. Michely, Europium underneath graphene on Ir(111): Intercalation mechanism, magnetism, and band structure Phys. Rev. B 90 2014 235437.
[124] L. Daukiya, M.N. Nair, S. Hajjar-Garreau, F. Vonau, D. Aubel, J.L. Bubendorff, M. Cranney, E. Denys, A. Florentin, G. Reiter, L. Simon, Highly n-doped graphene generated through intercalated terbium atoms, Phys. Rev. B 97 (2018), 035309.
[125] P. Rosenzweig, H. Karakachian, S. Link, K. Küster, U. Starke, Tuning the doping level of graphene in the vicinity of the Van Hove singularity via ytterbium intercalation, Phys. Rev. B 100 (2019), 035445.
[126] J. Kim, P. Lee, M. Ryu, H. Park, J. Chung, Cerium-induced changes in the π-band of graphene, RSC Adv. 6 (115) (2016) 114219–114223.

[127] K.M. Doebrich, A. Bostwick, J.L. McChesney, K. Rossnagel, E. Rotenberg, G. Kaindl, Fermi-Surface Topology and Helical Antiferromagnetism in Heavy Lanthanide Metals, Phys. Rev. Lett. 104 (2010), 246401.
[128] S.R. Power, F.S.M. Guimaraes, A.T. Costa, R.B. Muniz, M.S. Ferreira, Dynamic RKKY interaction in graphene, Phys. Rev. B 85 (2012), 195411.
[129] I.I. Klimovskikh, M.M. Otrokov, V.Yu. Voroshnin, D. Sostina, L. Petaccia, G. Di Santo, S. Thakur, E.V. Chulkov, A.M. Shikin, Spin-Orbit Coupling Induced Gap in Graphene on Pt(111) with Intercalated Pb Monolayer, ACS Nano 11 (1) (2017) 368–374.
[130] X. Fei, L. Zhang, W. Xiao, H. Chen, Y. Que, L. Liu, K. Yang, S. Du, H.-J. Gao, Structural and Electronic Properties of Pb- Intercalated Graphene on Ru(0001), J. Phys. Chem. C 119 (18) (2015) 9839–9844.
[131] A.M. Afzal, K.H. Min, B.M. Ko, J. Eom, Observation of giant spin–orbit interaction in graphene and heavy metal heterostructures, RSC Adv. 9 (54) (2019) 31797–31805.
[132] T.W. Hu, Q.L. Fang, X.H. Zhang, X.T. Liu, D.Y. Ma, R. Wei, K.W. Xu, F. Ma, Enhanced n-doping of epitaxial graphene on SiC by bismuth, Appl. Phys. Lett. 113 (2018), 011602.
[133] F. Calleja, H. Ochoa, M. Garnica, S. Barja, J.J. Navarro, A. Black, M.M. Otrokov, E.V. Chulkov, A. Arnau, A.L. Vázquez de Parga, F. Guinea, R. Miranda, Spatial variation of a giant spin–orbit effect induces electron confinement in graphene on Pb islands, Nat. Phys. 11 (1) (2015) 43–47.
[134] A.M. Alsharari, M.M. Asmar, S.E. Ulloa, Topological phases and twisting of graphene on a dichalcogenide monolayer, Phys. Rev. B 98 (2018), 195129.